Calculations of nonlinear spectra of liquid Xe. I. Third-order Raman response

Jianshu Cao,[a] Jianlan Wu, and Shilong Yang
Department of Chemistry, Massachusetts Institute of Technology, Cambridge, Massachusetts 02139

(Received 11 July 2001; accepted 30 November 2001)

The microscopic interactions and dynamics probed by third-order Raman spectroscopy in an atomic liquid (Xe) are explored within the Drude oscillator model, both numerically and analytically. Many-body polarization effects reduce the coefficient of the effective dipole–induced-dipole tensor. The isotropic part of the effective dipole–induced-dipole tensor arises primarily from the three-body interaction and is short-ranged. With an isotropic sample, the Raman response in any polarization geometry can be rigorously decomposed into an isotropic component and an anisotropic component, which primarily measure the strength and evolution of the two-body and three-body interactions, respectively. An interesting result from our analysis is the derivation of the standard mode-coupling equation for the intermediate scattering function and the mode-coupling equation for the bilinear density mode using Gaussian factorization of the memory kernel and the mean spherical approximation of the direct correlation function. The initial moment expansion along with the Gaussian factorization scheme allows us to predict the temporal profile of the Raman response function with reasonable accuracy. Furthermore, the Kirkwood superposition scheme approximates the Raman correlation function with pair distribution functions and time correlation functions and allows us to predict the ratio of the pair, three-particle, and four-particle contributions. These results, though obtained for Xe, are generally helpful in interpreting third-order spectroscopies of other liquids. [DOI: 10.1063/1.1445745]

I. INTRODUCTION

Advance in multiple-pulse Raman and infrared techniques has provided new tools for exploring molecule interactions in chemical and biological systems. The theory of frequency-domain Raman experiments has a long tradition, and its applications to condensed phase systems are described by Berne and Pecora.[1] Interest in liquids and mixtures has recently been revived by time-resolved fifth-order Raman and vibrational spectroscopies, which hold the promise of discriminating the inhomogeneous distribution of coherent motions against the homogeneous dynamics resulting from mode–mode couplings.[2–7] In a third-order Raman experiment, a pair of ultrafast light pulses excite a vibrational mode at time zero, and the Raman scattering is detected at time *t*. The third-order nonlinear spectrum is equivalent to the Fourier transform of the linear absorption spectrum.[8] In a fifth-order Raman experiment, a pair of ultrafast light pulses excite a vibrational mode at time zero, another pair of ultrafast light pulses perturb the motion at time t_1, thus amplifying the in-phase motion and suppressing the out-of-phase motion, and the Raman scattering is detected at time t_1+t_2. Mukamel, Loring, Tanimura, and Cho were the first theorists to explore the use of nonlinear Raman spectroscopy for the study of the coherence and coupling in condensed phase systems.[8–13] Though first fifth-order Raman experiments have been successfully demonstrated in molecular liquids and mixtures,[14–23] nonlinear Raman experiments can also be performed in atomic liquids. Atomic liquids provide a clean system where the dynamic response is due to the interparticle motion and is not contaminated by the reorientational motion of individual particles. In addition, our calculations of the Raman response function of Xe reveal general features shared by molecular liquids. These considerations motivate our detailed analysis of third-order Raman spectroscopy of Xe in this paper and fifth-order Raman spectroscopy of Xe in the companion paper. Some background and related work are summarized as follows.

(1) *Many-body polarization*. Since the polarizability of isolated atoms is isotropic, the scattering is of purely Rayleigh intensity and is not depolarized. In 1968, McTaugue and Birnbaum observed so-called collision-induced light scattering in dense rare gases Kr and Ar.[24] Early experimental and theoretical studies of depolarized light scattering signal from spherical molecules were summarized by Gelbart.[25] In the presence of binary collisions, two atoms form a transient diatomic molecule bond, which results in a vibrational mode with an induced diatomic polarizability.[26] The Raman signal in rare gases arises from many-body induced polarization effects. The effects of dipole–induced-dipole interactions on dielectric response and orientational relaxation of polar fluids were studied by Deutch, Wertheim, and Wolynes, among other theorists.[27–32] Similar many-body polarization effects in light scattering of molecular liquids were also explored by Ladanyi and Keyes, Madden, Tildesley, Steele, etc.[33–36] In Sec. II, we model many-body polarization effects with the Drude oscillator model, which consists of oscillatory dipoles interacting with the dipole–induced-dipole (DID) tensor.[37–40] The many-body effect on individual

[a]Electronic mail: jianshu@mit.edu

Drude oscillators leads to an enhanced value for the atomic polarizability, i.e., the renormalized polarizability. This enhanced polarizability has been derived within the mean spherical approximation by Pratt and, independently, by Hoye and Stell.[41,42] In order to calculate the effects of many-body polarization on Raman spectra, we use a simple resummation scheme in Appendix B to derive the renormalized atomic polarizability and, more importantly, the renormalized DID interaction tensor. Hence, we are able to reduce the many-body polarization to the effective one-body polarizability and two-body dipole–dipole tensor in Eq. (2.11).

(2) *Polarization selectivity*. Multiple pulse photoexcitation experiments are often carried out with different sequences of light polarization so that scattering intensities at different polarization geometries can be used to probe orientational dynamics. A well-known example is the third-order off-resonant Raman experiment, where the anisotropic component of the total polarizability, measured with the depolarization geometry, can be well-separated from the isotropic component of the total polarizability, observed along the magic angle.[1,43,44] Polarization selectivity is usually examined within the orientational diffusion model, which is adequate for molecular liquids with large rotational friction. Similar results can be obtained with other approaches including the instantaneous normal mode method. However, for atomic liquids, orientational relaxation is associated with the transient interparticle bond but not with single-particle reorientational motions, rendering the diffusion model inapplicable. Thus, in Sec. III, we formulate a general treatment of polarization selectivity using the isotropic symmetry of the sample and the tensor property of the dipole–dipole interaction.

(3) *Gaussian factorization and mode coupling equations*. Dynamic decomposition schemes have been widely used in the theoretical studies of solvation dynamics, energy relaxation and dephasing, charge transfer, etc.[45–48] One such scheme invokes the Gaussian factorization of density fluctuations at different times. The equilibrium distribution broken by the factorization approximation is partly reconstructed by incorporating the liquid distribution function. In the spirit of the mean spherical approximation, the direct pair correlation function is approximated by the product of the pair correlation function and the interaction potential. The Gaussian factorization scheme is shown in Sec. IV C to recover the standard mode coupling theory (MCT) equation for the intermediate scattering function derived by Götze *et al.*[49–51] Further, in Sec. IV D, we derive mode-coupling equations for four-point time correlation functions in a similar way and demonstrate that the resulting mode coupling equation is consistent with the hydrodynamic limit of the four-point correlation function. This justifies the simple Gaussian evaluation of the third-order Raman correlation function in the long-time limit.

(4) *Temporal profile of the response function*. In general, linear absorption spectra in liquids consist of a featureless peak broadened by various liquid modes. The third-order Raman spectrum is no exception in that its response function exhibits a simple peak along the time axis. This seemingly simple temporal profile is the result of the evolution of the total polarizability in liquids. Early theoretical studies of the depolarized light scattering spectrum were carried out by Madden and Ladd, Litovitz, and Montrose[52,53] and were summarized in Ref. 54. The instantaneous normal mode (INM) method provides a new approach to analyzing liquid and solvation dynamics.[55–59] In particular, Fourkas, Keyes, and their co-workers have employed the INM method to analyze the third-order and fifth-order liquid spectra.[60–62] Direct numerical calculations of the temporal profile of third-order and fifth-order response functions were carried out by Ma and Stratt on liquid Xe[63] and by Jansen, Snijders, and Duppen on CS_2.[64] Various theoretical treatments were introduced to calculate spectral line-broadenings and solvation dynamics.[65–72] Motivated by these works, in Sec. IV, we apply dynamic decomposition to the evaluation of the correlation function of the total polarizability. The initial behavior of the response function is fit to a Gaussian function with the first few moments, and is extended to longer times by Gaussian factorization of the four-point correlation function into a product of linear hydrodynamic modes.[50] In Sec. V, the correlation function for the total polarizability tensor is separated into the two-particle, three-particle, and four-particle contributions. These contributions are evaluated with the help of Kirkwood superposition and are approximated in terms of two-body equilibrium averages and two-body time-correlation functions. We analyze the relative contributions from these terms and confirm the predicted ratio of the three contributions in the long-time limit.[53]

The paper is organized according to the above-posed issues, with supporting derivations presented in the appendices. Our analysis is verified by numerical simulations, with the details described in Appendix C, and the numerical results are presented in relevant sections.

II. DRUDE OSCILLATOR MODEL AND ITS RENORMALIZATION

The relevant microscopic information in the third-order Raman experiment is described by the linear response function

$$R(t) = -\langle\{\mathbf{\Pi}(t), \mathbf{\Pi}(0)\}\rangle = -\beta \dot{C}(t), \tag{2.1}$$

where β is the inverse temperature, $\{\ \}$ is the Poisson bracket, and $C(t) = \langle \mathbf{\Pi}(t)\mathbf{\Pi}(0)\rangle$ is the time correlation function. The total Raman polarizability of the sample $\mathbf{\Pi}$ is a second-rank tensor in three-dimensional Cartesian space, and the response function and the correlation function are fourth-rank tensors in three-dimensional Cartesian space. The tensor elements describe Raman intensity profiles in various polarization geometries.

To calculate the total polarizability of liquid Xe, we introduce the Drude oscillator model, which consists of oscillating dipoles interacting through the second-order dipole tensor $\mathbf{T}$. The mean square fluctuation of an isolated Drude dipole is α/β with α the atomic polarizability. In this model, the total polarizability tensor of a fluid composed of N identical spherical Drude oscillators is

$$\mathbf{\Pi}(t) = \sum_{ij}^{N} \alpha[\mathbf{I} - \alpha \mathbf{T}(t)]_{ij}^{-1}, \tag{2.2}$$

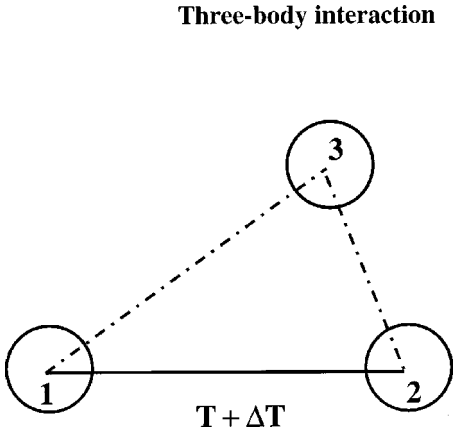

FIG. 1. Schematic of the three-body polarization effect. The solid line represents the dipole–dipole interaction between particles 1 and 2 with a fixed separation, the dashed lines represent intermediate interactions being integrated.

where the summation is carried over all pairs of particles, and $\mathbf{\Pi}$ is a function of the evolving liquid configuration through the coordinate dependence in $\mathbf{T}_{ij}(t)=\mathbf{T}[\mathbf{r}_{ij}(t)]$. The dipole–dipole interaction tensor is defined as

$$T_{\mu\nu}(\mathbf{r})=\frac{3r_\mu r_\nu-\delta_{\mu\nu}r^2}{r^5}=\frac{1}{r^3}D_{\mu\nu}(\hat{\mathbf{r}}), \tag{2.3}$$

where μ and ν denote the three Cartesian coordinates, $\mathbf{r}$ is the vector connecting a pair of liquid particles, $\hat{\mathbf{r}}=\mathbf{r}/r$ is the corresponding unit vector, and $\mathbf{D}$ is the traceless dimensionless tensor $\mathbf{D}(\hat{\mathbf{r}})=3\hat{\mathbf{r}}\hat{\mathbf{r}}-\mathbf{I}$.

A key issue in studying the polarizability spectrum of liquids is the induced many-body polarization. The many-body induced polarizability in atomic liquids is expanded as an infinite expansion in terms of $\mathbf{T}$,

$$\mathbf{\Pi}=\sum_{ij}\ \alpha\mathbf{I}\delta_{ij}+\alpha\mathbf{T}_{ij}\alpha+\alpha\mathbf{T}_{ik}\alpha\mathbf{T}_{kj}\alpha+\cdots, \tag{2.4}$$

where the repeated indices are summed implicitly. The first term in Eq. (2.4) is a constant for atomic liquids and hence will be ignored in dynamic calculations. The leading order truncation of $\mathbf{\Pi}$ results in the pair interaction approximation

$$\mathbf{\Pi}\approx\sum_{i}\ \alpha+\sum_{i\neq j}\ \alpha\mathbf{T}_{ij}\alpha, \tag{2.5}$$

where the first term is a constant and the second term corresponds to the first-order dipole–induced-dipole interaction (DID). Because $\mathbf{T}$ is a traceless tensor, the pair interaction in Eq. (2.5) is the anisotropic part of the DID polarizability with a time-dependent magnitude. The lack of the isotropic polarizability component in the pair interaction fails to explain the Raman intensity observed at the magic angle.

To account for the isotropic DID polarizability, it is necessary to include the next term in the expansion of Eq. (2.4), $\alpha^3\mathbf{T}_{ik}\mathbf{T}_{kj}$, as shown in Fig. 1. When $i=j$, this term contributes to the diagonal element and adds to the atomic polarizability

$$\Delta\alpha=\alpha^3\sum_j\ \mathbf{T}_{ij}\mathbf{T}_{jk}\alpha^3\rho\int d\mathbf{r}\,g(\mathbf{r})\mathrm{Tr}\frac{\mathbf{T}(\mathbf{r})^2}{3}d\mathbf{r}$$

$$=2\alpha^3\rho\int\frac{g(r)}{r^6}d\mathbf{r}, \tag{2.6}$$

which is an average over the pair distribution function $g(r)$. When $i\neq j$, this term contributes to the off-diagonal element and adds to the dipole–dipole interaction

$$\Delta\mathbf{T}_{12}=\alpha\rho\int d\mathbf{r}_3\,g(\mathbf{r}_1,\mathbf{r}_2,\mathbf{r}_3)/g(\mathbf{r}_{12})\mathbf{T}(\mathbf{r}_{13})\mathbf{T}(\mathbf{r}_{32})$$

$$\approx\Delta T_D(r_{12})\mathbf{D}(\hat{\mathbf{r}}_{12})+\Delta T_I(r_{12})\mathbf{I}, \tag{2.7}$$

where the anisotropic component ΔT_D and the isotropic component ΔT_I are expressed explicitly in Appendix A. Combining Eqs. (2.6) and (2.7), we arrive at a new form of the total Raman polarizability,

$$\mathbf{\Pi}\approx\sum_{i}\ (\alpha+\Delta\alpha)\mathbf{I}+\sum_{i\neq j}\ \alpha(\mathbf{T}_{ij}+\Delta\mathbf{T}_{ij})\alpha, \tag{2.8}$$

which incorporates the three-body dipole–dipole interaction. To leading order, two atoms form a transient molecular bond through the dipole–induced-dipole interaction and give rise to the anisotropic DID polarizability, whereas the three-body polarization effect leads to the isotropic DID polarizability and additional atomic polarizability.

In Appendix A, we explicitly evaluate ΔT_D and ΔT_I in Eq. (2.8) for a dilute hard-sphere system, where the pairwise correlation function is a step function $g(r)=0$ for $r\leqslant a$ and $g(r)=1$ for $r\geqslant a$, with a the hard-sphere diameter. After a lengthy calculation in Appendix A, we obtain

$$\Delta T_I(r)=\begin{cases}0, & r\geqslant 2a\\ \dfrac{\alpha\rho\pi}{6a^3}\left(\dfrac{r}{a}-2\right)^2\left(\dfrac{r}{a}+4\right), & r<2a\end{cases}, \tag{2.9}$$

where the interaction vanishes at $r\geqslant 2a$. Thus, the effective isotropic DID interaction is a short-range interaction, and the corresponding correlation function decays relatively fast initially. Similarly, we have from Appendix A

$$\Delta T_D(r)=\begin{cases}-\dfrac{4\pi\alpha\rho}{3r^3}, & r\geqslant 2a\\ -\dfrac{\pi\alpha\rho}{24a^3}\left(\dfrac{6a^2r-r^3}{a^3}\right), & r<2a\end{cases}, \tag{2.10}$$

which is also a stepwise function. The long-range effect of this term is to reduce the effective dipole–dipole interaction strength by $-4\pi\alpha\rho/3$, which is independent of the hard-sphere radius. These results will change as the liquid density increases but remain a good guide for understanding three-body polarization effects.

Following the same spirit, the higher-order many-body polarization terms in Eq. (2.4) can modify the atomic polarizability and pair interaction. In Appendix B, the expansion is explicitly re-summed to obtain a set of self-consistent equations for the renormalized polarizability $\bar{\alpha}$ and dipole tensor $\mathbf{T}$. The renormalized dipole propagator has both a traceless anisotropic part and a diagonal isotropic part $\mathbf{T}$

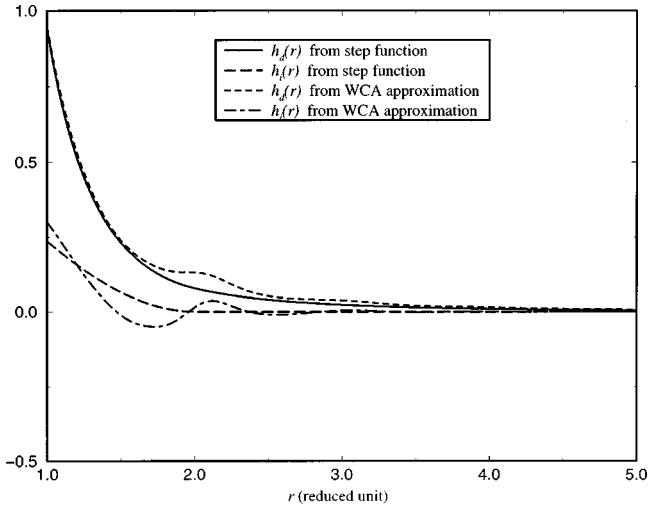

FIG. 2. A plot of the renormalization anisotropic and isotropic radial functions $h_D(r)$ and $h_I(r)$ calculated from the renormalization equation described in Appendix C and from the three-body terms with a step function for the pair correlation function. The Xe liquid is at reduced temperature $T^*=0.75$ and reduced density $\rho^*=0.85$.

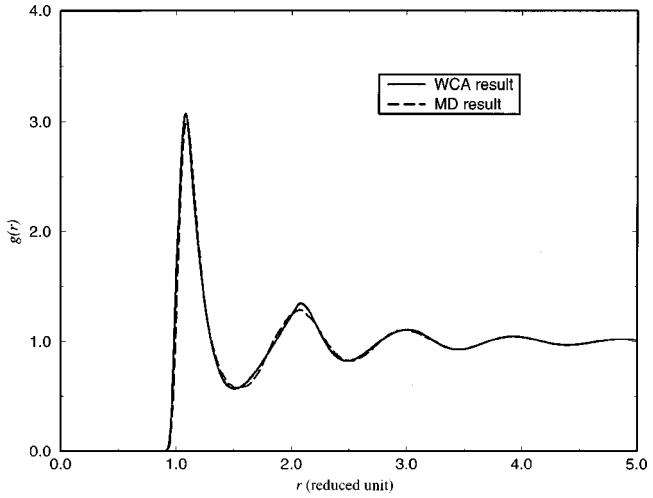

FIG. 3. A comparison of the exact pair correlation from the simulation and the WCA approximation used in the renormalization equation for Fig. 2.

$=h_I\mathbf{I}+h_D\mathbf{D}$ where the explicit expressions for h_D and for h_I are derived in Appendix B. The introduction of the renormalized quantities reduces the total polarizability tensor to

$$\mathbf{\Pi}\approx\sum_i \bar{\alpha}+\sum_{i\neq j}\bar{\alpha}\bar{\mathbf{T}}_{ij}\bar{\alpha}, \tag{2.11}$$

which now serves as the basis for further calculations.

Since the measured quantities are the correlation function and the response function, taking the thermal average on the level of the polarizability tensor ignores the dynamic effect of the integrated atoms in the expansion. In deriving Eqs. (2.8) and (2.11), the average of the dynamic trajectories of the integrated atoms in the expansion reduces the possible error, and we believe that the three-body averaging and renormalization procedure are reliable in this study.

An example. As the first example, we explicitly calculate the effective pair Raman polarizability for liquid Xe, both from the analytical solutions in Appendix B and from the three-body term in Appendix A. The pair potential for Xe atoms is the Lennard-Jones potential with parameters given in Appendix C, and thermal state of the Xe liquid is taken as temperature $T^*=0.75$ and density $\rho^*=0.85$, in reduced units. The three-body corrections—Eqs. (2.9) and (2.10)—are evaluated for a step function with an optimal radius taken from the WCA procedure. The resulting $h_I(r)$ and $h_D(r)$ are plotted in Fig. 2 and are shown to predict the approximate magnitudes of the many-body effects but fail to reproduce the structures seen in renormalized results. This difference is mainly due to the short-range order in the liquid Xe structure, which is not captured in the step function. We next apply the WCA correlation function and evaluate the self-consistent equation derived in Appendix B. The effective $\mathbf{T}$ thus obtained is plotted in Fig. 2 and is compared with the three-body results. In Fig. 3, the WCA pair correlation function is compared with the result from molecular dynamics (MD) simulation, and the two curves are found to be nearly identical in range of concern. Thus, the effective pair DID tensor can be accurately obtained by solving the renormalization equation with the WCA pair correlation function as the input.

To examine temperature and density effects, we calculate the two effective DID tensor components $h_D(r)$ and $h_I(r)$ for several densities in Fig. 4 and for several temperatures in Fig. 5. The solution follows the same procedure as described for Fig. 2. The contributions of the many-body effect in Figs. 4 and 5 increase with the liquid density and decrease with the liquid temperature. The many-body effects can be observed from the positions and amplitudes of the oscillations of $\Delta h_D(r)$ and $h_I(r)$. Evidently, the density dependence of the effective DID tensor is strong, whereas the temperature dependence is relatively weak. Since the increase in thermal velocity with temperature will be a dominant effect on liquid dynamics, the temperature dependence of the effective DID tensor does not necessarily correspond to the temperature dependence of the Raman correlation function.

III. POLARIZATION SELECTIVITY

The response function $R(t)$ is known as the third-order polarization, whose symmetry properties are well-studied. In an isotropic sample, twenty-one tensor elements are nonzero and only three elements are distinct for the third-order Raman experiment (R_{zzzz}, R_{zzyy}, and $R_{zyzy}=R_{zyyz}$). The rotational symmetry $R_{zzzz}=R_{zzyy}+R_{zyzy}+R_{zyyz}$ leaves two independent elements, which will be calculated in this paper.

Within the renormalized DID approximation, the correlation function is expressed as

$$C(t)=\left\langle\left(\sum_{ij}\bar{\alpha}\bar{\mathbf{T}}_{ij}(t)\bar{\alpha}\right)\left(\sum_{kl}\bar{\alpha}\bar{\mathbf{T}}_{kl}(0)\bar{\alpha}\right)\right\rangle$$
$$=\bar{\alpha}^4\int d\mathbf{r}\int d\mathbf{r}'\,\bar{\mathbf{T}}(\mathbf{r})P(\mathbf{r},\mathbf{r}',t)\bar{\mathbf{T}}(\mathbf{r}'), \tag{3.1}$$

where $P(\mathbf{r},\mathbf{r}',t)$ is the reduced joint probability distribution function (PDF) for finding a pair of liquid particles with relative displacement $\mathbf{r}$ at time zero and a pair of liquid par-

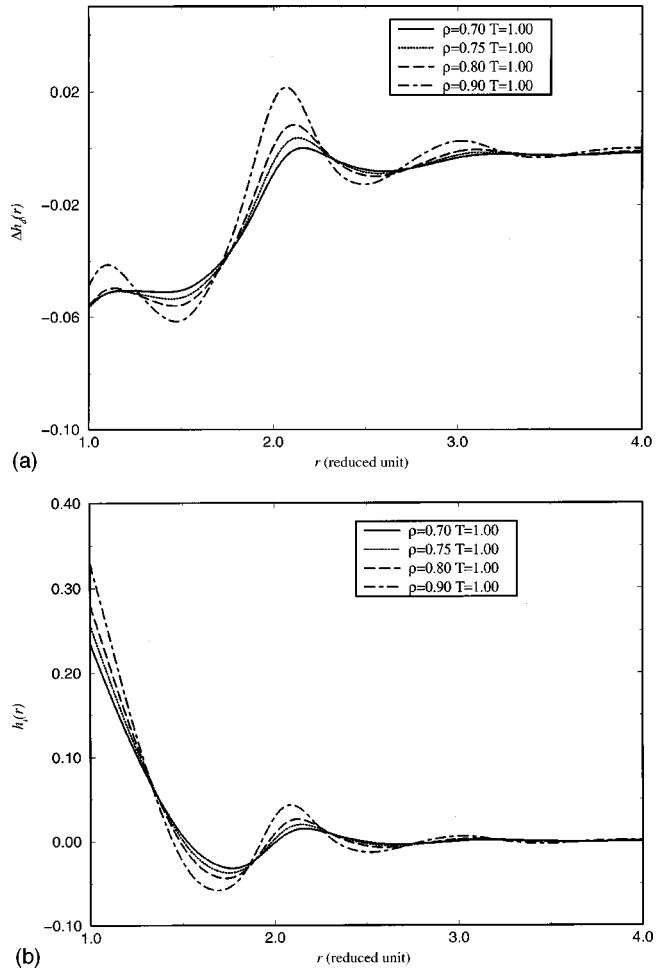

FIG. 4. A plot of the renormalized anisotropic and isotropic radial functions (a) $\Delta h_D(r)$ and (b) $h_I(r)$, for a set of densities at a fixed temperature.

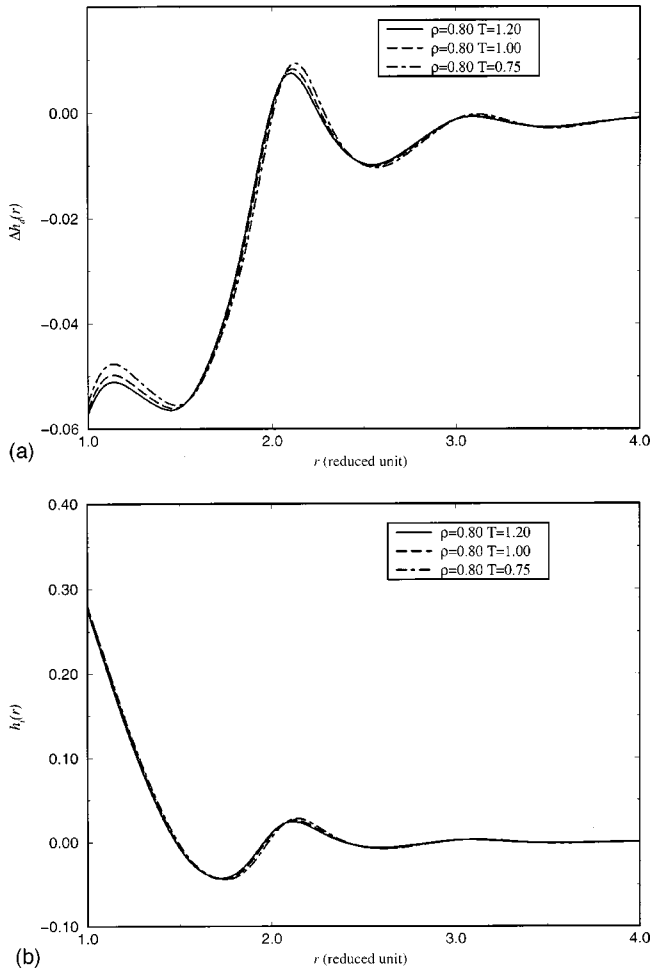

FIG. 5. A plot of the renormalized anisotropic and isotropic radial functions (a) $\Delta h_D(r)$ and (b) $h_I(r)$, for a set of temperatures at a fixed density.

ticles with relative displacement $\mathbf{r}'$ at time t. For an isotropic homogeneous liquid, the joint probability distribution function is expanded as

$$P(\mathbf{r},\mathbf{r}',t)=\left(\frac{1}{4\pi}\right)\sum_{lmm'} Y_{lm}(\hat{\mathbf{r}})P_{lmm'}(r,r',t)Y^*_{lm'}(\hat{\mathbf{r}}')$$
$$=\left(\frac{1}{4\pi}\right)\sum_{lm} Y_{lm}(\hat{\mathbf{r}})P_l(r,r',t)Y^*_{lm}(\hat{\mathbf{r}}'), \qquad (3.2)$$

where Y_{lm} is the spherical harmonic function. The symmetry of isotropic liquids removes the m-dependence in the radial part, i.e., $P_{lmm'}=P_l\delta_{m,m'}$. Thus, substituting Eq. (3.2) into Eq. (3.1), we have

$$C(t)=\left(\frac{1}{4\pi}\right)\overline{\alpha}^4\sum_m\left[\int Y_{2m}(\hat{\mathbf{r}})D(\hat{\mathbf{r}})d\hat{\mathbf{r}}\right]$$
$$\times\left[\int Y^*_{2m}(\hat{\mathbf{r}}')D(\hat{\mathbf{r}}')d\hat{\mathbf{r}}'\right]$$
$$\times\left[\int dr\int dr'\, r^2h_D(r)P_2(r,r',t)(r')^2h_D(r')\right]$$
$$+\left(\frac{1}{4\pi}\right)\overline{\alpha}^4\left[\int Y_{00}(\hat{\mathbf{r}})I(\hat{\mathbf{r}})d\hat{\mathbf{r}}\right]$$
$$\times\left[\int Y_{00}(\hat{\mathbf{r}}')I(\hat{\mathbf{r}}')d\hat{\mathbf{r}}'\right]$$
$$\times\left[\int dr\int dr'\, r^2h_I(r)P_0(r,r',t)(r')^2h_I(r')\right], \qquad (3.3)$$

where the first term is the contribution from the isotropic DID polarizability, the second term is the contribution from the anisotropic DID polarizability, and the cross term vanishes due to the tensor symmetry. Both terms can be factorized as an angular part, which depends on the polarization geometry, and a time-dependent radial part, which depends on the dipole–dipole interaction potential. From Eq. (3.3), three independent components of the third-order polarization tensor can be evaluated, giving

$$C_{zzzz}(t)=\tfrac{4}{5}C_{\text{aniso}}(t)+C_{\text{iso}}(t),$$
$$C_{zzyy}(t)=-\tfrac{2}{5}C_{\text{aniso}}(t)+C_{\text{iso}}(t), \qquad (3.4)$$
$$C_{zyzy}(t)=\tfrac{3}{5}C_{\text{aniso}}(t),$$

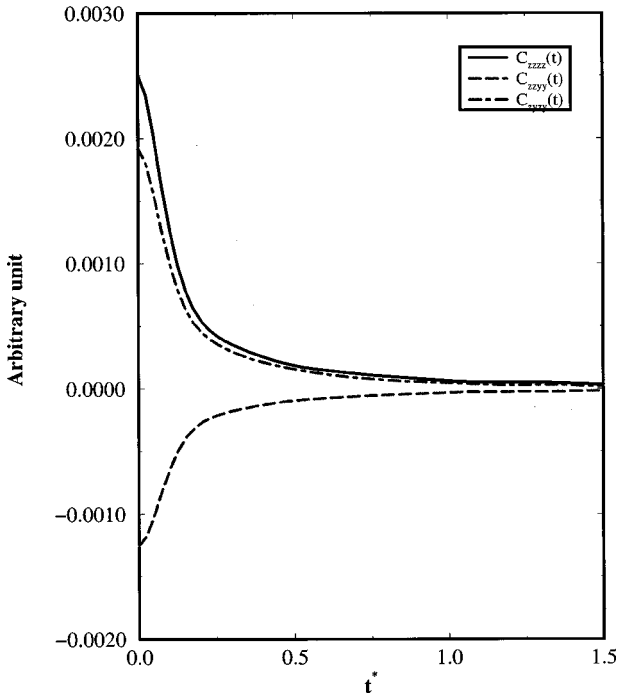

FIG. 6. A plot of the three elements of the third-order Raman correlation function obtained from numerical simulations of liquid Xe. The total polarizability tensor Π is calculated with the pair interaction approximation in Eq. (2.5). The simulation box consists of 108 Xe particles interacting with the Lennard-Jones potential at the reduced temperature of $T^*=0.75$ and the reduced density of $\rho^*=0.85$.

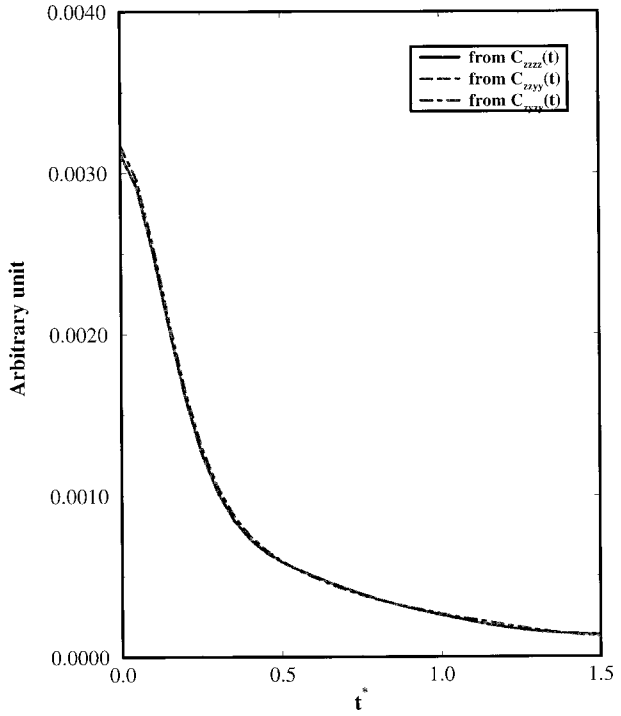

FIG. 7. A plot of the three tensor elements in Fig. 6 scaled according to the ratio 4:−2:3 as discussed in Sec. III. The scaled curves all fall on the same master curve.

where the symmetry relation $C_{zzzz}=C_{zyzy}+C_{zyyz}+C_{zzyy}$ is rigorously satisfied. Here, the anisotropic component obtained in the depolarized Raman intensity is given by

$$C_{\mathrm{aniso}}(t) = \overline{\alpha}^4\left\langle \sum_{ij} h_D[r_{ij}(0)]P_2[\mathbf{r}_{ij}(0)\mathbf{r}_{kl}(t)]\sum_{kl} h_D[r_{kl}(t)]\right\rangle, \tag{3.5}$$

whereas the isotropic component obtained from the Raman intensity at the magic angle is given by

$$C_{\mathrm{iso}}(t)=\overline{\alpha}^4\left\langle \sum_{ij} h_I[r_{ij}(0)]\sum_{kl} h_I[r_{kl}(t)]\right\rangle, \tag{3.6}$$

where P_l is the lth order Legendre polynomial. The polarization dependence in the above-given expressions is similar to those derived for the rotational diffusion model or obtained from the INM analysis. The essential difference is that for an atomic fluid the transient dipole is formed by at least two atoms. Hence, the anisotropic polarizability is independent of the liquid density to leading order, and the isotropic polarizable is proportional to the liquid density.

In a dilute sample, the dipole interaction in Eq. (3.4) has only the anisotropic component, so that the second term $C_{\mathrm{iso}}(t)$ can be ignored. As a result, the intensity ratios of the three independent polarization components remain constant,

$$C_{zzzz}(t):C_{zzyy}(t):C_{zyzy}(t)=4:-2:3, \tag{3.7}$$

which is the same relation obtained for isolated molecules or diffusing molecules. In fact, this relation is general and rigorous for any traceless tensor, because the first ratio is imposed by the zero-trace identity $C_{zzzz}+C_{zzyy}+C_{zzxx}=0$ and the second ratio is imposed by the rotational symmetry. As the liquid density increases, these ratios are contaminated by the contribution from the isotropic part of the DID polarizability and are no longer constant. The intensity at the magic angle is due to the isotropic part and has a different time-dependence from the anisotropic part.

The above-given analysis is independent of the type of liquids, the form of interaction potentials, or the description of particle motions. In general, the symmetry of the polarizability tensor $\mathbf{\Pi}$ completely characterizes the decomposition of the Raman spectrum into independent polarization components. Since the third-order polarization has two independent components, we truncate or renormalize the many-body polarization to the pair interaction form with a second-rank tensor. To isolate more independent tensor components, we have to resort to two-dimensional experiments, which can be performed with more polarization geometries and thus have higher selectivity (see Paper II).

As a numerical example, we calculated the third-order Raman correlation function $C(t)$ for liquid Xe. The simulation details and the molecular model are described in Appendix C. First, we employed the pair interaction approximation of the total polarizability tensor, $\Pi=\Sigma\alpha\mathbf{T}\alpha$, which yields the anisotropic component of the Raman intensity. Figures 6 and 7 show that the three components of the correlation function, $C_{zzzz}(t)$, $C_{zyzy}(t)$, and $C_{zzyy}(t)$, follow the ratio 4:3:−2 within computational errors. There, the three tensor elements of liquid Xe were calculated with the full expression for the total polarizability tensor Π in Eq. (2.2), including both the isotropic and anisotropic DID polarizabilities. As shown in

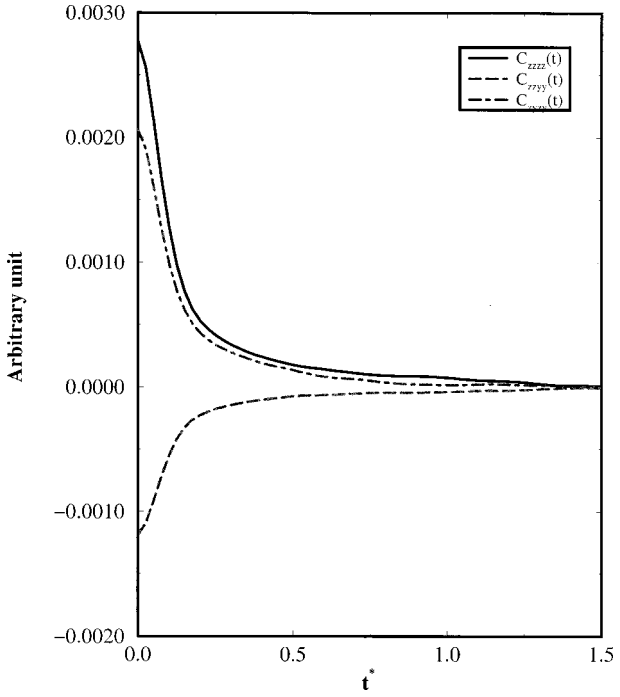

FIG. 8. A plot of the three elements of the third-order Raman correlation function for simulated liquid Xe, where Π is the full polarizability tensor in Eq. (2.2). The thermodynamic conditions and simulation details are the same as in Fig. 6.

Fig. 8, $C_{zzzz}(t)$ and $C_{zzyy}(t)$ are modified by an isotropic component, and the absolute intensity of C_{zyzy} increases as we include all the higher order DID interactions. In Fig. 9, the anisotropic component $C_{\text{aniso}}(t)$ and the isotropic component $C_{\text{iso}}(t)$ are decomposed from $C_{zzzz}(t)$, $C_{zzyy}(t)$, and $C_{zyzy}(t)$ as

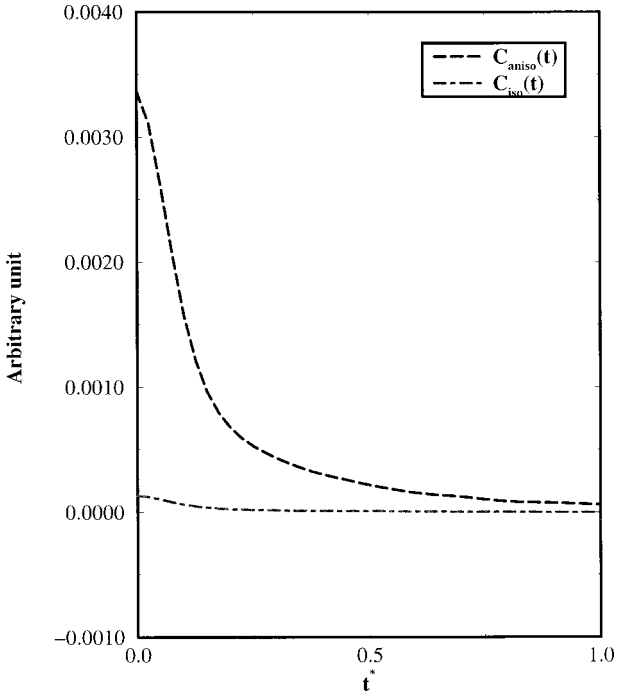

FIG. 9. A plot of the anisotropic and the isotropic contributions decomposed from $C_{zzzz}(t)$, $C_{zzyy}(t)$, and $C_{zyzy}(t)$ in Fig. 8.

$$C_{\text{iso}}=\tfrac{1}{3}[C_{zzzz}(t)+2C_{zzyy}(t)],$$
$$C_{\text{aniso}}=\tfrac{5}{12}[C_{zzzz}(t)-C_{zzyy}(t)+2C_{zyzy}(t)]. \tag{3.8}$$

As expected, the isotropic component is smaller than the anisotropic component, with the ratio of $C_{\text{iso}}(0)/C_{\text{aniso}}(0)$ around 0.1. Since $C_{\text{iso}}(0)/C_{\text{aniso}}(0)\approx h_i^2/h_d^2$, this ratio is consistent with the estimation of the ratio of the two components of the effective DID tensor, h_i/h_d, in Sec. II. In fact, direct numerical integration of Eqs. (16) and (17) shows that the anisotropic response C_{aniso} is one magnitude larger than the isotropic response $C_{\text{iso}}(t)$, which agrees very well with our direct simulation of the full dipole–dipole interaction tensor.

IV. MOLECULAR HYDRODYNAMICS CALCULATIONS

A. Initial behavior: Gaussian fitting

The goal of molecular hydrodynamics calculations is to predict Raman response from equilibrium properties and other experimental measurements. Given the zero value of the response function at the initial time and the exponential decay at long times, the response has a maximal in between. The maximal in the response function is mainly due to the initial behavior and thereby can be predicted based on moment expansion. The Taylor expansion of the time correlation function $C(t)=\Sigma_n(-1)^n c_{2n}t^{2n}/(2n)!$ is defined by the even moment $c_{2n}=\langle \mathbf{\Pi}^{(n)}\mathbf{\Pi}^{(n)}\rangle$. We assume a Gaussian functional form for the response function

$$\chi(t)=-ct\exp\left(-\gamma\frac{t^2}{2}\right), \tag{4.1}$$

where the two coefficients can be fitted to the second and fourth moments $c=c_2$ and $\gamma=c_4/(3c_2)$. Hence, the maximal of the response function occurs at $t_m=1/\sqrt{\lambda}$.

For simplicity, we evaluate the two moments for the simple case of the two-body interaction with the bare dipole–dipole interaction, $\Pi=\alpha^2\Sigma_{ij}T_{ij}$. With only the anisotropic contribution, the different polarizations maintain a fixed ratio, so that we need only the R_{zzzz} component. The first moment is given by

$$c_2=\sum_{\mu}\langle\partial_\mu T_{zz}\partial_\mu T_{zz}\rangle v_0^2=12v_0^2\int\frac{g(r)}{r^6}d\mathbf{r} \tag{4.2}$$

and the fourth moment is given by

$$c_4=\sum_{\mu\nu}\langle[\partial_\mu\partial_\nu T v_\mu v_\nu+\partial_\mu T F_\mu/m]^2\rangle$$
$$=3\sum_{\mu\nu}V^4\langle\partial_\mu\partial_\nu T\partial_\mu\partial_\nu T\rangle+v_0^2\langle\partial_\mu\partial_\nu\Omega_{ij}^2\rangle, \tag{4.3}$$

where $\Omega_{ij}^2=\partial_i\partial_j U/m$ is the curvature and $v_0^2=k_BT/m$. These moments are evaluated explicitly in Appendix D, and the predicted temporal profile is compared favorably with numerical simulations in Fig. 10.

We notice that the integrated Raman intensity is given by the initial value of the correlation function, i.e.,

$$\int_0^\infty R(t)dt=-\beta C(0), \tag{4.4}$$

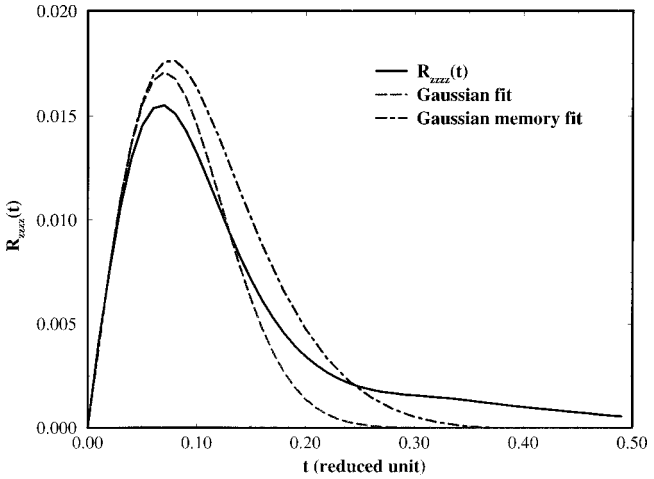

FIG. 10. A comparison of the anisotropic component $C_{zyzy}(t)$ from molecule dynamics simulation, from the Gaussian approximation of the response function, and from the Gaussian fitting of the memory function.

where $C(0)=\langle \mathbf{IIII} \rangle$ can be easily evaluated. Thus, the integrated intensity imposes an additional constraint on the functional fitting of the response function.

Another fitting is to start with the generalized Langevin equation (GLE) for the total polarizability tensor

$$\dot{C}(t)=-\int_0^t M(\tau)C(t-\tau)d\tau, \tag{4.5}$$

where $M(t)$ is the memory kernel. The response function can be solved in Laplace space, giving

$$\hat{\chi}(s)=-\beta[s\hat{C}(s)-C(0)]=\beta C(0)\frac{\hat{M}(s)}{s+\hat{M}(s)}, \tag{4.6}$$

which, via numerical inversion of Laplace transform, gives the time dependence of the response function $\chi(t)$. The memory kernel can be fitted to a Gaussian function

$$M(t)=c_M \exp(-\gamma_M t^2), \tag{4.7}$$

where the coefficients are related to the initial moments of the correlation function as $c_M=c_2/c_0$ and $\gamma_M=(c_4-c_2^2/c_0)$. The Laplace transform of the Gaussian memory kernel is

$$\hat{M}(s)=\frac{M_0}{2}\sqrt{\frac{\pi}{\alpha}}\exp\left(\frac{s^2}{4\alpha}\right)\left[-1+\mathrm{erf}\left(\frac{s}{2\sqrt{\alpha}}\right)\right], \tag{4.8}$$

which is used in Eq. (4.6) to yield the response function. As seen from Fig. 10, both Gaussian fitting procedures predict the peak in the response function with reasonable accuracy, but fail to reproduce the long-time slow decay. Thus, we conclude the peak response of the Raman signal is due to the inertial motion in liquids.

B. Direct Gaussian factorization

In the hydrodynamic limit, correlation functions can be expressed in terms of collective hydrodynamic modes in liquids. A simple way to establish this relationship is the Gaussian factorization scheme, which treats liquid densities at different times as Gaussian variables and maintains thermal equilibrium by incorporating equilibrium distribution functions for the initial and final configurations. Formally, our Gaussian scheme can be expressed as

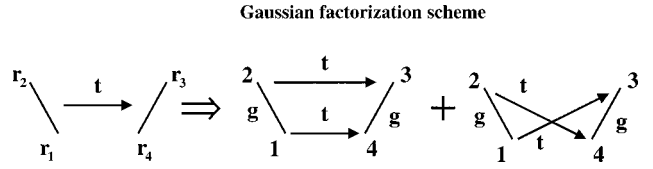

FIG. 11. Schematic of the Gaussian factorization of the four-point density correlation function. The evolution of joint liquid densities at $\mathbf{r}_1$ and $\mathbf{r}_2$ is factorized into the product of the propagation of single particle density. The equilibrium condition of the liquid densities at $\mathbf{r}_1$ and $\mathbf{r}_2$ at time zero is imposed by the pair correlation function, and the same equilibrium condition is imposed for the two liquid densities at time t.

$$\lim_{t\to\infty}\langle \rho(\Gamma,t)\rho(\Gamma',0)\rangle = g(\Gamma)g(\Gamma')\Pi_{\mathbf{r}\in\Gamma\mathbf{r}'\in\Gamma'}G(\mathbf{r},\mathbf{r}',t), \tag{4.9}$$

where Γ and Γ' represent the initial and final configurations, respectively, and $\mathbf{r}$ and $\mathbf{r}'$ are coordinates in the initial and final configurations. The Gaussian factorization scheme can be justified based on the central limit theorem and is applicable to long-time large-displacement motions in the hydrodynamic limit. This simple scheme has appeared in literature in various forms and contexts. For example, in Appendix E, the force correlation function is decomposed into density correlation functions, and the resulting expression has been used by Banchi, Cherayil, Fayer, and their co-workers for calculating vibrational relaxation rate.[47,48]

We now apply the Gaussian factorization scheme to calculate the third-order Raman response function. To begin, the polarizability tensor is written in Fourier space as

$$\begin{aligned}\Pi &= \sum_{i\neq j}\bar{\alpha}\bar{\mathbf{T}}_{ij}\bar{\alpha}=\frac{\bar{\alpha}^2}{V}\sum_{\mathbf{k}}\sum_{i\neq j}\bar{\mathbf{T}}(\mathbf{k})e^{i\mathbf{k}(\mathbf{r}_i-\mathbf{r}_j)}\\ &= \frac{\bar{\alpha}^2}{V}\sum_{\mathbf{k}}\bar{\mathbf{T}}(\mathbf{k})\rho(\mathbf{k})\rho^*(\mathbf{k}),\end{aligned} \tag{4.10}$$

where $\rho(\mathbf{k})=\Sigma_i \exp(-i\mathbf{k}\mathbf{r}_i)$ is the number density. In Eq. (4.10), the term with $i=j$ is excluded by setting the dipole interaction to zero whenever the internuclear distance vanishes, $\bar{\mathbf{T}}_{i=j}=0$. Substituting this expression into the correlation function of the total polarizability, we have

$$\begin{aligned}C(t) &= \frac{1}{V^2}\bar{\alpha}^4\left\langle \sum_{\mathbf{k}}\bar{\mathbf{T}}(\mathbf{k})\rho(\mathbf{k},t)\rho^*(\mathbf{k},t)\right.\\ &\quad\times\left.\left|\sum_{\mathbf{k}'}\bar{\mathbf{T}}(\mathbf{k}')\rho(\mathbf{k}',0)\rho^*(\mathbf{k}',0)\right\rangle\right.\\ &\approx 2N\rho\bar{\alpha}^4\frac{1}{(2\pi)^3}\int d\mathbf{k}\bar{\mathbf{T}}_g(\mathbf{k})\bar{\mathbf{T}}_g(\mathbf{k})F^2(\mathbf{k},t),\end{aligned} \tag{4.11}$$

where $F(\mathbf{k},t)$ is the intermediate scattering function. In Eq. (4.11), $T_g(\mathbf{r})=T(\mathbf{r})g(\mathbf{r})$ is the dipole interaction operator dressed by the pairwise distribution function. The essential step in the derivation of Eq. (4.11) is the Gaussian factorization of the density fluctuation, illustrated in Fig. 11 and explicitly expressed as

$$\langle \rho(\mathbf{r}_1,t)\rho(\mathbf{r}_2,t)|\rho(\mathbf{r}_3,0)\rho(\mathbf{r}_4,0)\rangle \approx g(\mathbf{r}_1-\mathbf{r}_2)g(\mathbf{r}_3-\mathbf{r}_4) \times[G(\mathbf{r}_1-\mathbf{r}_3,t)G(\mathbf{r}_2-\mathbf{r}_4,t) + G(\mathbf{r}_2-\mathbf{r}_3,t)G(\mathbf{r}_1-\mathbf{r}_4,t)], \quad (4.12)$$

where the equilibrium term does not contribute at long times. Evaluation of the Gaussian factorization expression requires numerical simulations or viscoelastic approximations for $F(\mathbf{k},t)$.[73–75] Balucani and Zoppi have discussed Eq. (4.11) extensively and have found reasonable agreement with the experimental depolarized data.[54]

Since the Fourier transformation preserves the order of the tensor, the intensity ratio of different polarizability geometries from the anisotropic contribution remains constant, and the intensity ratio of different polarizability configurations from the isotropic contribution remains constant. Thus the polarization dependence predicted by the hydrodynamic models is consistent with the previous analysis of polarization selectivity in Sec. III.

The initial behavior is not included in Eq. (4.11) because the Gaussian factorization is not applicable in the short time regime. The structure of the Raman response function is dominated by the features at relatively short time, so the initial value corrections to the direct Gaussian factorization can improve the accuracy of the scheme. To do this, we first derive the GLE, which incorporates the initial behavior through the frequency term, and apply Gaussian factorization to the memory function instead of the correlation function. Interestingly, this scheme is shown in the following to give the mode-coupling equation for the intermediate scattering function and the bilinear density fluctuation. Then, the simple Gaussian factorization in Eq. (4.11) is shown to be the hydrodynamic limit of the mode-coupling equation for $\rho(\mathbf{k})\rho(-\mathbf{k})$.

C. Mode coupling equation for the intermediate scattering function

We now demonstrate that the standard mode coupling equation for the intermediate scattering function $F(\mathbf{k},t)=\langle\rho(\mathbf{k},t)|\rho(\mathbf{k},0)\rangle$ can be easily derived with the Gaussian factorization scheme in combination with the mean spherical approximation. The starting point is the generalized Langevin equation (GLE) with two variables $\rho(\mathbf{k})$ and $\dot{\rho}(\mathbf{k})$, which leads to a reduced GLE for the density fluctuation

$$\ddot{F}(\mathbf{k},t)+\omega^2 F(\mathbf{k},t)+\int_0^t M(\mathbf{k},t-\tau)F(\mathbf{k},\tau)d\tau=0. \quad (4.13)$$

Here, the effective frequency is defined as

$$\omega^2=\frac{\langle\dot{\rho}^2\rangle}{\langle\rho^2\rangle}=\frac{k^2v^2}{S(\mathbf{k})} \quad (4.14)$$

with $S(\mathbf{k})$ the structure factor and $v^2=k_BT/m$ the thermal velocity, and the memory kernel is defined as

$$M(\mathbf{k},t)=\frac{\langle\ddot{\rho}+\omega^2\rho|e^{-iQ\mathcal{L}t}|\ddot{\rho}+\omega^2\rho\rangle}{\langle\dot{\rho}^2\rangle}, \quad (4.15)$$

where $Q=1-P$ is the orthogonal projection operator, $\mathcal{L}$ is the Liouville operator, and the denominator is $\langle\dot{\rho}\dot{\rho}\rangle=Nv_0^2k^2$. The double time-derivative of the density operator is defined as the Fourier transform

$$\ddot{\rho}(\mathbf{k})=\left(\sum_i i\mathbf{k}\mathbf{v}_i e^{i\mathbf{k}\mathbf{r}_i}\right)' \approx \sum_i i\frac{\mathbf{k}\mathbf{F}_i}{m}e^{i\mathbf{k}\mathbf{r}_i} =\sum_{i\neq j} i\frac{\mathbf{k}}{m}[-\nabla\phi(\mathbf{r}_{ij})]e^{i\mathbf{k}\mathbf{r}_i} =\sum_{\mathbf{q}}\frac{1}{V}\frac{\mathbf{k}\mathbf{q}}{m}\phi(\mathbf{k})[\rho(\mathbf{q})\rho(\mathbf{k}-\mathbf{q})-N], \quad (4.16)$$

where $\phi(\mathbf{k})$ is the Fourier transform of the interaction potential and the higher order k^2 term is ignored. The application of the Gaussian factorization scheme to the relevant part of the memory kernel leads to

$$\langle\ddot{\rho}|e^{iQ\mathcal{L}t}|\ddot{\rho}\rangle=\frac{1}{V^2m^2}\sum_{\mathbf{q}}\sum_{\mathbf{q}'}(\mathbf{k}\mathbf{q})(\mathbf{k}\mathbf{q}')\phi(\mathbf{q})\phi(\mathbf{q}') \times\langle\rho(\mathbf{q})\rho(\mathbf{k}-\mathbf{q})|e^{iQ\mathcal{L}t}|\rho(\mathbf{q}')\rho(\mathbf{k}-\mathbf{q}')\rangle \approx\left(\frac{N}{Vm}\right)^2\sum_{\mathbf{q}}[(\mathbf{k}\mathbf{q})^2\phi_g(\mathbf{q})^2 \times F(\mathbf{q},t)F(\mathbf{k}-\mathbf{q},t)+(\mathbf{k}\mathbf{q})(\mathbf{k}^2-\mathbf{k}\mathbf{q}) \times\phi(\mathbf{q})_g\phi_g(\mathbf{k}-\mathbf{q})F(\mathbf{q},t) \times F(\mathbf{k}-\mathbf{q},t)], \quad (4.17)$$

where $\phi_g(\mathbf{r})=\phi(\mathbf{r})g(\mathbf{r})$ is the dressed interaction potential. Linearizing the Percus–Yevick closure leads to the following approximation:

$$c(\mathbf{r})=(1-e^{\beta\phi(\mathbf{r})})g(\mathbf{r})\approx-\beta\phi(\mathbf{r})g(\mathbf{r}), \quad (4.18)$$

where $c(\mathbf{r})$ is the direct solute–solvent correlation function. Replacing $-\beta\phi(\mathbf{r})g(\mathbf{r})$ with the direct correlation function $c(\mathbf{r})$ follows the same spirit as the mean spherical approximation. Further, we take the continuous limit of $\mathbf{k}$, and symmetrize the integrand. The resulting expression for the memory kernel is written as

$$M(\mathbf{k},t)=\frac{\rho k_BT}{2mk^2}\frac{1}{(2\pi)^3}\int d\mathbf{q}\,F(\mathbf{q},t)F(\mathbf{k}-\mathbf{q},t) \times[(\mathbf{k}\mathbf{q})c(\mathbf{q})+(\mathbf{k}^2-\mathbf{k}\mathbf{q})c(\mathbf{k}-\mathbf{q})]^2, \quad (4.19)$$

which is exactly the same expression derived with more complicated mode coupling procedures.[49,51,76]

Combined with the mean spherical approximation for the direct correlation function, the Gaussian factorization approach provides a simple and intuitive alternative to the formalism of mode coupling theory and helps one understand the underlying assumptions involved in the mode coupling approximation. Equation (4.12) applies to the long-time large-displacement motion, but does not recover the equilibrium distribution. For low-temperature glasses, where the system is not completely ergodic, the dynamic decomposition scheme has to be modified to incorporate dynamic heterogeneities observed on the experimental time scale.

Our derivation of the mode-coupling equation for the intermediate scattering function is simple but approximate. About the same time as our derivation, a more rigorous treatment was obtained by Zaccarelli *et al.*[77] They related the Newtonian equation for the liquid density to the generalized Langevin equation for $F(\mathbf{k},t)$ as in Eq. (4.13), and then exploited the fluctuation-dissipation theorem to obtain an explicit expression for the memory kernel instead of the Mori–Zwanzig form for the memory kernel. Both the random phase approximation for the direct correlation function and the Gaussian factorization for multipoint time correlation functions were used to arrive at the mode-coupling equation for $F(\mathbf{k},t)$. Their derivation justifies the approximation for the direct correlation function from a dynamic perspective and reveals the self-consistent mean-field nature of the mode-coupling equation for $F(\mathbf{k},t)$. We will explore both Gaussian factorization and the more rigorous derivation in a future paper.

D. Mode-coupling equation for the bilinear density fluctuation

The Gaussian fitting of the third-order Raman response function is accurate for relatively short times but decays to vanishingly small value. Direct Gaussian factorization of the third-order response is valid only in the hydrodynamic regime. Now we explore a possible way to combine these two limits and obtain the mode-coupling equation of the Raman spectrum. As shown earlier, the Raman correlation function can be written as

$$C(t)=\frac{1}{V^2}\overline{\alpha}^4\Big\langle \sum_{\mathbf{k}} \overline{\mathbf{T}}(\mathbf{k})\rho(\mathbf{k},t)\rho^*(\mathbf{k},t) \times\Big|\sum_{\mathbf{k}'} \overline{\mathbf{T}}(\mathbf{k}')\rho(\mathbf{k}',0)\rho^*(\mathbf{k}',0)\Big\rangle \approx \frac{2}{V^2}\overline{\alpha}^4\sum_{\mathbf{k}} \overline{\mathbf{T}}(\mathbf{k})\overline{\mathbf{T}}(\mathbf{k})\langle Q_1(\mathbf{k},t)Q_1(\mathbf{k},0)\rangle, \tag{4.20}$$

where $Q_1(\mathbf{k},t)=\rho(\mathbf{k},t)\rho(-\mathbf{k},t)$ is the bilinear density mode, and the correlation between different wave vectors is ignored.[78] Unlike the linear density mode, there is no hydrodynamic equation to describe the bilinear mode. Direct Gaussian decomposition reduces the four-point correlation function to

$$\langle Q_1(\mathbf{k},t)Q_1(\mathbf{k},0)\rangle \approx N^2F^2(\mathbf{k},t), \tag{4.21}$$

which recovers the hydrodynamic expression, Eq. (4.11). As shown in the early derivation, applying the Gaussian factorization to the memory kernel in GLE leads to a simple way to obtain the mode-coupling equation. Here, we derive the mode-coupling equation for the bilinear mode $Q_1(\mathbf{k},t)$ and justify the direct Gaussian factorization as its long-time solution.

To begin, a three-element basis set $\underline{Q}$ is defined as $Q_1=\rho(\mathbf{k})\rho(-\mathbf{k})$, $Q_2=\rho(\mathbf{k})P(-\mathbf{k})+\rho(-\mathbf{k})P(\mathbf{k})$, and $Q_3=P(\mathbf{k})P(-\mathbf{k})$, where $P(\mathbf{k})$ is the momentum density function (i.e., the longitudinal current), $P(\mathbf{k})=\Sigma_i P_{ik}\exp(i\mathbf{k}\mathbf{r_i})$, $P_{ik}=\mathbf{P}_i\hat{\mathbf{k}}$, and $\hat{\mathbf{k}}$ is the unit vector in the $\mathbf{k}$ direction. Here, a simplified hydrodynamic approach is used in constructing the basis set, in which the temperature fluctuation is ignored.[52,73] Within this basis set, we can write the GLE using the Mori projection operator defined as $\mathcal{P}=\langle\cdots Q^+\rangle\cdot\langle QQ^+\rangle^{-1}Q$. A complete mode-coupling description includes the projection onto different $\mathbf{k}$ wave vectors. Following the argument of Keyes and Oppenheim,[78] the most important contribution arises from the diagonal parts. To simplify the calculation, we consider only the diagonal contributions in the derivation of GLE, giving

$$\begin{pmatrix}\dot{Q}_1(t)\\ \dot{Q}_2(t)\\ \dot{Q}_3(t)\end{pmatrix}=i\begin{pmatrix}0 & \Omega_{12} & 0\\ \Omega_{21} & 0 & \Omega_{23}\\ 0 & \Omega_{32} & 0\end{pmatrix}\begin{pmatrix}Q_1(t)\\ Q_2(t)\\ Q_3(t)\end{pmatrix} -\begin{pmatrix}K_{11} & K_{12} & K_{13}\\ K_{21} & K_{22} & K_{23}\\ K_{31} & k_{32} & K_{33}\end{pmatrix}*\begin{pmatrix}Q_1\\ Q_2\\ Q_3\end{pmatrix}+\begin{pmatrix}f_1(t)\\ f_2(t)\\ f_3(t)\end{pmatrix}, \tag{4.22}$$

where the asterisk $(*)$ stands for the time convolution, i.e., $A*B=\int_0^t A(t-\tau)B(\tau)d\tau$. Using the $\underline{N}$-ordering method[78] and the Gaussian factorization approximation, these frequencies are given as

$$\Omega_{12}=\frac{k}{m},\quad \Omega_{21}\simeq\frac{2k}{\beta S(k)},\quad \Omega_{23}\simeq\frac{2k}{m},\quad \Omega_{32}\simeq\frac{k}{\beta S(k)}, \tag{4.23}$$

where $S(k)$ is the static structure factor. In Eq. (2.1), vector $f(t)$ represents the fluctuation force defined as $f(t)=e^{i(1-\mathcal{P})\mathcal{L}t}(1-\mathcal{P})\dot{Q}$, matrix $K(t)$ represents the memory kernel, given by $K(t)=\langle f(t)f^+\rangle\cdot\langle QQ^+\rangle^{-1}$. Using the same approximation for expressing $\ddot{\rho}(\mathbf{k})$, the initial value of the fluctuation force $f(0)$ becomes

$$\begin{pmatrix}f_1(0)\\ f_2(0)\\ f_3(0)\end{pmatrix}=\frac{im}{k}\begin{pmatrix}0\\ \sum_q \mathbf{k}\cdot\mathbf{q}\phi_g^2(q)[\rho(\mathbf{k}-\mathbf{q})\rho(\mathbf{q})\rho(-\mathbf{k})+\rho(\mathbf{q}-\mathbf{k})\rho(-\mathbf{q})\rho(\mathbf{k})]/(mV)-2\omega_k^2Q_1\\ \sum_q \mathbf{k}\cdot\mathbf{q}\phi_g^2(q)[\rho(\mathbf{k}-\mathbf{q})\rho(\mathbf{q})P(-\mathbf{k})+\rho(\mathbf{q}-\mathbf{k})\rho(-\mathbf{q})P(\mathbf{k})]/(mV)-\omega_k^2Q_2\end{pmatrix}, \tag{4.24}$$

where only the linear term of $\mathbf{k}$ is kept. Following a conventional approach, we replace the operator $e^{i(1-\mathcal{P})\mathcal{L}t}$ with the full time propogator $e^{i\mathcal{L}t}$, and then use the fluctuation–dissipation relation to derive the expression for the memory kernel $K(t)$. We apply two approximations in our calculation: the Gaussian factorization, which is assumed to be valid for the long-time memory kernel, and the mean spherical approximation (MSA),[77] $c(k)\approx-\beta\phi_g(k)$, used in the derivation of the mode coupling equation for $\rho(\mathbf{k},t)$. Thus, the three nonzero elements are given by

$$
\begin{aligned}
K_{22}(t) &\simeq \frac{\rho}{mk^2\beta}\frac{1}{(2\pi)^3}\int d\mathbf{q}\, C(\mathbf{k},\mathbf{q})F(\mathbf{k}\\
&\quad -\mathbf{q},t)F(\mathbf{q},t)F(\mathbf{k},t),\\
K_{31}(t) &\simeq \frac{2\rho}{3S(k)k^2\beta^2}\frac{1}{(2\pi)^3}\int d\mathbf{q}\\
&\quad \times C(\mathbf{k},\mathbf{q})F(\mathbf{k}-\mathbf{q},t)F(\mathbf{q},t)\Phi(\mathbf{k},t), \qquad (4.25)\\
K_{33}(t) &\simeq \frac{4\rho}{3mk^2\beta}\frac{1}{(2\pi)^3}\int d\mathbf{q}\\
&\quad \times C(\mathbf{k},\mathbf{q})\Phi(\mathbf{k}-\mathbf{q},t)\Phi(\mathbf{q},t)\Phi(\mathbf{k},t),
\end{aligned}
$$

where $C(\mathbf{k},\mathbf{q})=c(\mathbf{q})^2(\mathbf{k}\cdot\mathbf{q})^2+c(\mathbf{q})c(\mathbf{k}-\mathbf{q})[\mathbf{k}\cdot(\mathbf{k}-\mathbf{q})]$, F is the density correlation function (intermediate scattering function), $F(\mathbf{k},t)=\langle\rho_k(t)\rho_{-k}(0)\rangle/N$, and Φ is the moment correlation function (logitudinal current correlation function), $\Phi(\mathbf{k},t)=\beta\langle P_k(t)P_{-k}(0)\rangle/Nm$. Madden derived a similar result, but he did not incorporate the dynamics of mode-coupling effects.[52] Equations (4.22) and (4.25) relate the four-point correlation functions to the linear density fluctuation. Some of the approximations used are not necessary, and a more rigorous derivation of the mode-coupling equation is presented in a future paper by Wu and Cao.

In principle, if the frequencies and memory kernels are known, the correlation functions can be solved for a given set of initial conditions from Eq. (4.25). Here, instead of numerical calculations, we use the mode-coupling equation to justify the direct Gaussian factorization expression of the four-point density correlation function. We begin by writing Eq. (4.22) explicitly as

$$
\begin{aligned}
\dot{Q}_1(t) &= i\frac{k}{m}Q_2(t),\\
\dot{Q}_2(t) &= i\frac{2k\beta}{m^2S(k)}Q_1(t)+i\frac{2k}{m}Q_3(t)-K_{22}*Q_2+f_2(t),\\
\dot{Q}_3(t) &= i\frac{2k\beta}{m^2S(k)}Q_2(t)-K_{31}*Q_1-K_{33}*Q_3(t)+f_3(t),
\end{aligned}
\qquad (4.26)
$$

which yields the first-, second-, and third-order differential equations for $\langle Q_1(t)Q_1(0)\rangle$. Direct Gaussian factorization of the three basis-set elements yield $\langle Q_1(0)Q_1(t)\rangle\approx N^2F^2(t)$, $\langle Q_2(0)Q_2(t)\rangle\approx 2N^2F(t)\Phi(t)$, $\langle Q_3(0)Q_3(t)\rangle\approx N^2\Phi(t)\Phi(t)$, and cross terms. These approximate relations can be shown to satisfy the first-order and second-order time differential equations exactly, and the third-order time differential equation approximately, when the mode-coupling equations for $F(t)$ and $\Phi(t)$ are used. In other words, the direct Gaussian factorization of the four-point density correlation function is consistent with the long-time solution to the mode-coupling equation in Eq. (4.26), thus justifying the hydrodynamic limit of the third-order Raman response function.

V. PAIR, TRIPLET, AND QUADRUPLET CONTRIBUTIONS

An alternative to Gaussian factorization is the dynamic Kirkwood superposition approximation, which decomposes many-body time correlation functions into pair quantities. The Gaussian factorization scheme is based on liquid densities in space, whereas the dynamic Kirkwood decomposition is based on particles with specified identities. For example, Skinner and co-workers have used the approximation to develop a molecular theory for condensed phase spectroscopy[45,46] (see Appendix E). Here, we use a similar approach to evaluate the contributions from two particles (pair), three particles (triplet), and four particles (quadruplet) to third-order Raman correlation function.

A. Two-particle contribution

With the renormalized DID interaction in Eq. (2.11), the time-dependent part of the correlation function can be decomposed as $C(t)=\langle\boldsymbol{\Pi}(t)\boldsymbol{\Pi}(0)\rangle=C_2(t)+C_3(t)+C_4(t)$, where $C_n(t)$ is the n-particle contribution. These terms are explicitly given as

$$
\begin{aligned}
C_2(t) &= 2\overline{\alpha}^4\sum_{i\neq j}\overline{\mathbf{T}}_{ij}(t)\overline{\mathbf{T}}_{ij}(0)\\
&= 2N(N-1)\overline{\alpha}^4\langle\overline{\mathbf{T}}_{12}(t)\overline{\mathbf{T}}_{12}\rangle, \qquad (5.1)\\
C_3(t) &= 4\overline{\alpha}^4\sum_{i\neq j\neq k}\overline{\mathbf{T}}_{ij}(t)\overline{\mathbf{T}}_{jk}(0)\\
&= 4N(N-1)(N-2)\overline{\alpha}^4\langle\overline{\mathbf{T}}_{12}(t)\overline{\mathbf{T}}_{23}(0)\rangle, \qquad (5.2)\\
C_4(t) &= \sum_{i\neq j\neq k\neq l}\overline{\alpha}^4\mathbf{T}_{ij}(t)\mathbf{T}_{kl}(0)\\
&= N(N-1)(N-2)(N-3)\overline{\alpha}^4\langle\overline{\mathbf{T}}_{12}(t)\overline{\mathbf{T}}_{34}(0)\rangle,
\end{aligned}
\qquad (5.3)
$$

where the total number of interaction pairs adds up to $N^2(N-1)^2$.

For simplicity, we first calculate the two-particle contribution to the time-correlation function of the total polarizability

$$
\begin{aligned}
C_2(t) &= 2\overline{\alpha}^4\int d\mathbf{r}_1\int d\mathbf{r}_2\int d\mathbf{r}_1'\int d\mathbf{r}_2'\,\overline{\mathbf{T}}(\mathbf{r}_{12})\\
&\quad\times P_0(\mathbf{r}_1,\mathbf{r}_2,\mathbf{r}_1',\mathbf{r}_2',t)\overline{\mathbf{T}}(\mathbf{r}_{12}'), \qquad (5.4)
\end{aligned}
$$

where P_0 is the joint PDF for finding two particles at $\mathbf{r}_1$ and $\mathbf{r}_2$ initially and then the same particles at $\mathbf{r}_1'$ and $\mathbf{r}_2'$ at a later time t. The two sets of coordinates are transformed into relative coordinates $\mathbf{r}=\mathbf{r}_1-\mathbf{r}_2$ and $\mathbf{r}'=\mathbf{r}_1'-\mathbf{r}_2'$ and the center of mass coordinates $\mathbf{r}_c=(\mathbf{r}_1+\mathbf{r}_2)/2$ and $\mathbf{r}_c'=(\mathbf{r}_1'+\mathbf{r}_2')/2$, so that $P_0=P_{\text{c.m.}}(\mathbf{r}_c,\mathbf{r}_c',t)P_{\text{rel}}(\mathbf{r},\mathbf{r}',t)$. It is implied here that the

center-of-mass motion is decoupled from the relative motion so that the joint PDF is a function of relative coordinates only. Consequently, $C_2(t)$ becomes

$$C_2(t)=2\bar{\alpha}^4 N\int d\mathbf{r}\int d\mathbf{r}'\,\bar{\mathbf{T}}(\mathbf{r})P_{\rm rel}(\mathbf{r},\mathbf{r}',t)\bar{\mathbf{T}}(\mathbf{r}')$$
$$=2\bar{\alpha}^4 N\rho\int d\mathbf{r}\int d\mathbf{r}'\,\bar{\mathbf{T}}(\mathbf{r})g(\mathbf{r})G(\mathbf{r},\mathbf{r}',t)\bar{\mathbf{T}}(\mathbf{r}'), \tag{5.5}$$

which is identical to Eq. (5.4) with $P_0(t)=2NP_{\rm rel}(t)$. In Eq. (5.5), the joint probability of the relative coordinate is written as $P_{\rm rel}(\mathbf{r},\mathbf{r}',t)=\rho g(\mathbf{r})G(\mathbf{r},\mathbf{r}',t)$, where $g(\mathbf{r})$ is the equilibrium pair distribution function and $G(t)$ is the Green's function. The initial value of the Green's function is a delta function $G(\mathbf{r},\mathbf{r}',0)=g(\mathbf{r})\delta(\mathbf{r}-\mathbf{r}')$ so that the two expressions in Eqs. (5.1) and (5.5) are equivalent.

As an alternative, the exact expression in Eq. (5.5) can be rewritten as

$$C_2(t)=2N\bar{\alpha}^4\int d\mathbf{r}'\int d\mathbf{r}\int d\mathbf{r}_0\left[\frac{1}{(2\pi)^3}\int d\mathbf{k}\exp^{i\mathbf{k}(\mathbf{r}-\mathbf{r}_0)}\right]$$
$$\times g(\mathbf{r}_0)\bar{\mathbf{T}}(\mathbf{r}_0)G(\mathbf{r},\mathbf{r}',t)\bar{\mathbf{T}}(\mathbf{r}'), \tag{5.6}$$

where the Fourier transform of the delta function $\delta(\mathbf{r}-\mathbf{r}_0)$ is inserted. Then, with the equilibrium average $\langle A(\mathbf{r})\rangle=\rho\int d\mathbf{r}A(\mathbf{r})g(\mathbf{r})$ and the time-correlation function $\langle e^{i\mathbf{kr}(0)}\bar{\mathbf{T}}[r(t)]\rangle=\rho\int d\mathbf{r}\int d\mathbf{r}'g(\mathbf{r})e^{i\mathbf{kr}}G(\mathbf{r},\mathbf{r}',t)\bar{\mathbf{T}}(\mathbf{r}')$, we reduce Eq. (5.6) to

$$C_2(t)\approx 2V\bar{\alpha}^4\frac{1}{(2\pi)^3}\int d\mathbf{k}\langle e^{-i\mathbf{kr}}\bar{\mathbf{T}}(\mathbf{r})\rangle\langle e^{i\mathbf{kr}(0)}\bar{\mathbf{T}}[\mathbf{r}(t)]\rangle, \tag{5.7}$$

where $V=N/\rho$ is the volume and the approximation is due to the over-accounting of the pair distribution function $g(\mathbf{r})$. It turns out that this approximate form of $C_2(t)$ is consistent with the approximate expressions for $C_3(t)$ and $C_4(t)$ derived in the following.

B. Dynamic Kirkwood superposition

To proceed, we evaluate the three-particle contribution

$$C_3(t)=4\bar{\alpha}^4\int d\mathbf{r}_1\,d\mathbf{r}_2\,d\mathbf{r}_3\,d\mathbf{r}_1'\,d\mathbf{r}_2'\,d\mathbf{r}_3'\,\bar{\mathbf{T}}(\mathbf{r}_{12})$$
$$\times P_0(\mathbf{r}_1,\mathbf{r}_2,\mathbf{r}_3,\mathbf{r}_1',\mathbf{r}_2',\mathbf{r}_3',t)\bar{\mathbf{T}}(\mathbf{r}_{23}')$$
$$=4N\bar{\alpha}^4\int d\mathbf{r}_{12}\,d\mathbf{r}_{23}\,d\mathbf{r}_{12}'\,d\mathbf{r}_{23}'\,g(\mathbf{r}_1,\mathbf{r}_2,\mathbf{r}_3)$$
$$\times\bar{\mathbf{T}}(\mathbf{r}_{12})G(\mathbf{r}_{12},\mathbf{r}_{23},\mathbf{r}_{12}',\mathbf{r}_{23}',t)\bar{\mathbf{T}}(\mathbf{r}_{23}'), \tag{5.8}$$

where g is the three-body distribution function and G is the three-body Green's function with the initial condition $G(0)=\delta(\mathbf{r}_{12}-\mathbf{r}_{12}')\delta(\mathbf{r}_{23}-\mathbf{r}_{23}')$. Evidently, the integration over the coordinates other than $\mathbf{r}_{12}$ and $\mathbf{r}_{23}'$ leads to the reduced probability function P in Eq. (3.1) for the three-body contribution. To evaluate Eq. (5.8), the delta function $\delta(\mathbf{r}_{12}+\mathbf{r}_{23}+\mathbf{r}_{31})$ is inserted to constrain the initial triangular geometry with the additional coordinate $\mathbf{r}_{31}$. As illustrated in Fig. 12,

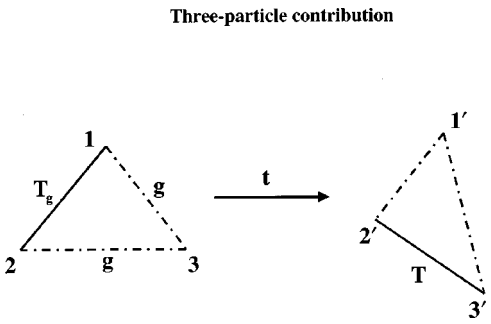

FIG. 12. Schematic of the dynamic Kirkwood superposition approximation for the three-body contribution to the polarizability tensor correlation function. The three-body propagation is approximated by the pair motion of particles, and the three-body equilibrium is maintained initially through the Kirkwood superposition.

we decompose the three-body distribution function as $g(\mathbf{r}_1,\mathbf{r}_2,\mathbf{r}_3)=g(\mathbf{r}_{12})g(\mathbf{r}_{23})g(\mathbf{r}_{31})$, and the three-body Green's function into the product of the two-body Green's functions, $G(\mathbf{r}_{12},\mathbf{r}_{23},\mathbf{r}_{12}',\mathbf{r}_{23}',t)=G(\mathbf{r}_{12},\mathbf{r}_{12}',t)G(\mathbf{r}_{23},\mathbf{r}_{23}',t)$. Consequently, the three-body contribution is factored

$$C_3(t)\approx 4N\bar{\alpha}^4\frac{1}{(2\pi)^3}\int d\mathbf{k}$$
$$\times\int d\mathbf{r}_{12}\,d\mathbf{r}_{23}\,d\mathbf{r}_{31}\,d\mathbf{r}_{12}'\,d\mathbf{r}_{23}'e^{i\mathbf{k}(\mathbf{r}_{12}+\mathbf{r}_{23}+\mathbf{r}_{31})}$$
$$\times g(\mathbf{r}_{12})g(\mathbf{r}_{23})g(\mathbf{r}_{31})$$
$$\times\bar{\mathbf{T}}(\mathbf{r}_{12})G(\mathbf{r}_{12},\mathbf{r}_{12}',t)G(\mathbf{r}_{23},\mathbf{r}_{23}',t)\bar{\mathbf{T}}(\mathbf{r}_{23}')$$
$$=4V\bar{\alpha}^4\frac{1}{(2\pi)^3}\int d\mathbf{k}\langle e^{i\mathbf{kr}}\rangle\langle e^{i\mathbf{kr}}\bar{\mathbf{T}}(\mathbf{r})\rangle$$
$$\times\langle e^{i\mathbf{kr}(0)}\bar{\mathbf{T}}[\mathbf{r}(t)]\rangle, \tag{5.9}$$

where the two-body functions are defined as in Eq. (5.7). The approximations involved can be viewed as an extension of the Kirkwood superposition to the dynamic regime.

Next, the four-particle contribution is rewritten as

$$C_4(t)=N\bar{\alpha}^4\int d\mathbf{r}_{12}\,d\mathbf{r}_{23}\,d\mathbf{r}_{34}\,d\mathbf{r}_{12}\,d\mathbf{r}_{23}'\,d\mathbf{r}_{34}'$$
$$\times g(\mathbf{r}_1,\mathbf{r}_2,\mathbf{r}_3,\mathbf{r}_4)\bar{\mathbf{T}}(\mathbf{r}_{12})$$
$$\times G(\mathbf{r}_{12},\mathbf{r}_{23},\mathbf{r}_{34},\mathbf{r}_{12}',\mathbf{r}_{23}',\mathbf{r}_{34}',t)\bar{\mathbf{T}}(\mathbf{r}_{34}'), \tag{5.10}$$

where g is the four-body distribution function and G is the four-body Green's function. Evidently, the integration over the coordinates other than $\mathbf{r}_{12}$ and $\mathbf{r}_{34}'$ leads to the reduced probability distribution function P in Eq. (3.1) for the four-body contribution. As illustrated in Fig. 13, we repeat the same procedure as in the derivation of Eq. (5.9), and factorize $C_4(t)$ into the product of two-body averages and two-body correlation functions as

$$C_4(t)\approx V\bar{\alpha}^4\frac{2}{(2\pi)^3}\int d\mathbf{k}\langle e^{i\mathbf{kr}}\rangle^2\langle e^{i\mathbf{kr}}\bar{\mathbf{T}}(\mathbf{r})\rangle$$
$$\times\langle e^{i\mathbf{kr}(0)}\bar{\mathbf{T}}[\mathbf{r}(t)]\rangle, \tag{5.11}$$

which differs from Eq. (5.9) only with a static factor $\langle e^{i\mathbf{kr}}\rangle$.

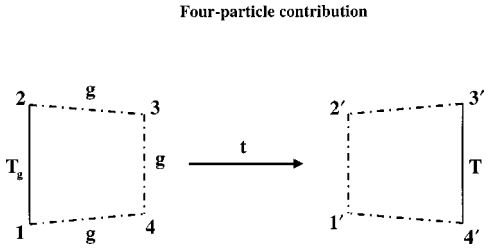

FIG. 13. Schematic of the dynamic Kirkwood superposition approximation for the four-body contribution to the polarizability tensor correlation function. The four-body propagation is approximated by the pair motion of particles, and the four-body equilibrium is maintained initially through an extension of the Kirkwood superposition.

Finally, combining Eqs. (5.7), (5.9), and (5.10) yields

$$C(t)=V\overline{\alpha}^4\frac{1}{(2\pi)^3}\int d\mathbf{k}(2+4\langle e^{i\mathbf{kr}}\rangle+2\langle e^{i\mathbf{kr}}\rangle^2)\times\langle e^{i\mathbf{kr}}\overline{\mathbf{T}}(\mathbf{r})\rangle\langle e^{i\mathbf{kr}(0)}\overline{\mathbf{T}}[\mathbf{r}(t)]\rangle, \tag{5.12}$$

where the relative weight of three contributions is approximately proportional to $\langle e^{i\mathbf{kr}(0)}\rangle$. Evidently, the two-particle, three-particle, and four-particle contributions have the same angular dependence, and the same time dependence in Fourier space but with different equilibrium weights. Using the spherical harmonics expansion, we explicitly calculate the two independent radial functions in Eq. (3.5) and in Eq. (3.6), giving

$$C_{\mathrm{aniso}}(t)=\frac{1}{(2\pi)^3}V\overline{\alpha}^4\int d\mathbf{k}(2+4\langle j_0(kr)\rangle+2\langle j_0(kr)\rangle^2)\langle h_D(r)j_2(kr)\rangle\times\langle j_2(kr)G_2(r,r',t)h_D(r')\rangle \tag{5.13}$$

and

$$C_{\mathrm{iso}}(t)=\frac{1}{(2\pi)^3}V\overline{\alpha}^4\int d\mathbf{k}(2+4\langle j_0(kr)\rangle+2\langle j_0(kr)\rangle^2)\times\langle h_I(r)j_2(kr)\rangle\langle j_0(kr)G_0(r,r',t)h_I(r')\rangle, \tag{5.14}$$

where all the quantities are two-body equilibrium averages and time-correlation functions.

The inherent structure in liquids leads to prominent peaks in the two-body distribution function and time-correlation function in Eqs. (5.13) and (5.14) such that the integral in Fourier space is dominated by these peaks. It then follows from Eqs. (5.13) and (5.14) that the contributions from the two-particle, three-particle, and four-particle terms share similar temporal profiles with the relative ratios determined by the static structure. In fact, by virtue of $\langle e^{i\mathbf{kr}}\rangle=S(k)-1$, we can rewrite Eq. (5.12) as

$$C(t)=V\overline{\alpha}^4\frac{2}{(2\pi)^3}\int d\mathbf{k}\{1+2[S(\mathbf{k})-1]+[S(\mathbf{k})-1]^2\}\times\langle e^{i\mathbf{kr}}\overline{\mathbf{T}}(\mathbf{r})\rangle\langle e^{i\mathbf{kr}(0)}\overline{\mathbf{T}}[\mathbf{r}(t)]\rangle \tag{5.15}$$

$$=V\overline{\alpha}^4\frac{2}{(2\pi)^3}\int d\mathbf{k}\,S(\mathbf{k})^2\langle e^{i\mathbf{kr}}\overline{\mathbf{T}}(\mathbf{r})\rangle\times\langle e^{i\mathbf{kr}(0)}\overline{\mathbf{T}}[\mathbf{r}(t)]\rangle, \tag{5.16}$$

where the ratios of the three contributions are related to the structure factor. For relatively large wave number, $S(\mathbf{k})$ becomes very small, so that the contributions follow the ratio: $C_2:C_3:C_4\approx 1:-2:1$. This ratio has been observed in numerical simulations and has been analyzed by Ladd *et al.*[53] Their analysis applies a similar dynamic decomposition but invokes free-particle diffusion instead of more general dynamic propagation G_2 and G_0, thus ignoring the different time dependencies between the depolarized component and the isotropic component.

In deriving Eq. (5.12), we have made several assumptions: (1) The center-of-mass motion is decoupled from the relative motion. (2) The geometric constraint on the many-body configuration is imposed only at the initial time. (3) The many-body distribution function and the many-body Green's function are decomposed in a similar way as the Kirkwood superposition approximation. These assumptions emphasize the central role of pairwise relative motions and local structures at short time scales but ignore possible collective motions. Nevertheless, the resulting expressions based on these assumptions allow us to understand and calculate many-particle contributions in terms of two-body properties.

C. Diffusion model

In general, the Green's function $G_l(t)$ decays faster as the angular momentum number l increases. We confirm this statement with the help of the diffusion equation

$$\frac{\partial G_l}{\partial t}=D\frac{1}{r^2}\frac{\partial}{\partial r}r^2\frac{\partial}{\partial r}G_l-D\frac{l(l+1)}{r^2}G_l+D\beta\frac{\partial}{\partial r}\left[\frac{\partial U}{\partial r}G_l\right], \tag{5.17}$$

where D is the diffusion constant for the relative motion between two Xe atoms. The potential of mean force is determined from $U(r)=-K_BT\ln[g(r)]$. Skinner and co-worker also used a generalized time variable to incorporate the initial behavior on the coarse-grained level. Equation (5.17) can be transformed into a Hermitian form and its time-dependent solution can be formally expanded as $G_l(r,r',t)=\Sigma_n\phi_{nl}(r)\phi_{nl}(r')\exp(-\lambda_{nl}t)$, where $\phi_{nl}(r)$ is the eigenfunction and λ_{nl} is the corresponding eigenvalue. The long-time exponential decay is dominated by the first nonzero eigenvalue λ_{1l}. Given the eigensolution for $l=0$, the eigenvalue for nonzero l can be evaluated via perturbation theory

$$\lambda_{ln}\approx\lambda_{0n}+Dl(l+1)\int\frac{\phi_{n0}^2(r)}{r^2}d\mathbf{r}, \tag{5.18}$$

which increases as a function of $l(l+1)$. Therefore, the intensity along the magic angle, associated with $G_0(t)$, decays slower than the intensity from the C_{xzxz} component, associated with $G_2(t)$. Though based on the diffusion model, we believe that this conclusion holds in general.

VI. CONCLUSIONS

To conclude, we summarize the main results in response to the issues raised in Sec. I.

(1) Within the Drude oscillator model, the leading term of the anisotropic part of the Raman response is determined by the two-body dipole–dipole tensor, whereas the leading term of the isotropic part of the Raman response is determined by the three-body dipole interaction. Higher order many-body polarization terms can be incorporated through a renormalization procedure. In comparison with the anisotropic part, the isotropic part of the effective dipole tensor has a short interaction range, thus resulting in a fast initial decay in the isotropic response of atomic liquids.

(2) The three distinct tensor elements in the third-order Raman response are decomposed into an isotropic component and an anisotropic component with the coefficients determined by the tensor properties of the dipole interaction. The decomposition does not only apply to integrated scattering intensity or the peak intensity but is also valid for all the time. Moreover, the polarization dependence obtained in this fashion is general in that it does not rely on the particular model of liquid dynamics or the type of liquids.

(3) The Gaussian factorization scheme treats liquid densities at different times as Gaussian variables and maintains the equilibrium distribution by imposing equilibrium distribution functions. This procedure combined with the mean spherical approximation for the direct correlation function allows us to recover the mode-coupling equations for the intermediate scattering function and the bilinear density correlation function. Another approach based on the dynamic Kirkwood superposition scheme decomposes the many-body time correlation function into pair quantities. Although both schemes can be understood as two possible realizations of dynamic decomposition of high-order time correlation functions, Gaussian factorization applies to density fluctuations in space, whereas dynamic Kirkwood superposition applies to particles in liquid.

(4) The two dynamic decomposition schemes are applied to the calculation of the third-order Raman response in Xe with several observations. (i) The two-particle, three-particle, and four-particle contributions to the Raman polarization have similar temporal profiles in Fourier space but with different amplitudes determined by the static structure. (ii) In dense liquids, the long-time decay of the isotropic component is slower than that of the anisotropic component. (iii) The Gaussian fitting according to initial moments gives a relatively good prediction of the response peak. (iv) The Gaussian factorization scheme leads to a simple hydrodynamic expression, which relates the Raman response to density fluctuations and predicts the dynamic response with reasonable accuracy.

These analytic results are compared favorably with numerical simulations and can be generalized to more complicated liquids. Future research will be devoted to the calculation of fifth-order spectra (see Paper II) as well as the modeling of nonlinear spectra of molecular liquids.

ACKNOWLEDGMENTS

The research is supported by the AT&T Research Fund Award, the Petroleum Research Fund administrated by the American Chemical Society, and the NSF Career Award (No. Che-0093210). We thank I. Oppenheim, D.R. Reichman, and A. Tokmakoff for discussions and comments.

APPENDIX A: THREE-BODY DIPOLE–DIPOLE INTERACTION IN THE DILUTE HARD-SPHERE MODEL

The many-body polarizability is expanded in terms of the dipole tensor $\mathbf{T}$ in Eq. (2.4), where the first term is the polarizability of individual atoms and the second term leads to the anisotropic part of the dipole–induced-dipole (DID) interaction. To account for the isotropic DID polarizability, we now evaluate the third term $\alpha^3 T_{i,k} T_{k,j}$. The diagonal element of this term $i=j$ adds to the atomic polarizability given by Eq. (2.6). The off-diagonal element of this term contributes to the dipole–dipole interaction

$$\Delta \mathbf{T}_{12} = \alpha\rho \int d\mathbf{r}_3\, g(\mathbf{r}_1,\mathbf{r}_2,\mathbf{r}_3)/g(\mathbf{r}_{12})\mathbf{T}(\mathbf{r}_{13})\mathbf{T}(\mathbf{r}_{32})$$

$$\approx \alpha\rho \int d\mathbf{r}_3\, g(\mathbf{r}_{13})g(\mathbf{r}_{32})\mathbf{T}(\mathbf{r}_{13})\mathbf{T}(\mathbf{r}_{32}), \tag{A1}$$

where the Kirkwood superposition approximation $g(\mathbf{r}_1,\mathbf{r}_2,\mathbf{r}_3)\approx g(\mathbf{r}_{12})g(\mathbf{r}_{23})g(\mathbf{r}_{31})$ is adopted. The radial function associated with the anisotropic polarizability is

$$\Delta T_D(r) = -\frac{\alpha\rho}{(2\pi)^3} \int d\mathbf{k}[q_2(k)]^2 j_2(kr), \tag{A2}$$

and the radial function associated with the isotropic polarizability is

$$\Delta T_I(r) = \frac{2\alpha\rho}{(2\pi)^3} \int d\mathbf{k}[q_2(k)]^2 j_0(kr), \tag{A3}$$

where j_l is the lth order spherical Bessel function and $q_2(k) = -\int j_2(kr) g(r)/r^3\, d\mathbf{r}$.

In this appendix, $\Delta T_D(r)$ and $\Delta T_I(r)$ are calculated for a dilute hard-sphere fluid. At the low-density limit, the pairwise correlation function $g(\mathbf{r})$ takes the form of the step function,

$$g(\mathbf{r}) = \begin{cases} 0, & r \leqslant a \\ 1, & r > a \end{cases}, \tag{A4}$$

where a is the diameter of the liquid molecule. The Fourier transform of the step function is given by

$$q_2(k) = 4\pi\left[\frac{\cos ka}{(ka)^2} - \frac{\sin ka}{(ka)^3}\right], \tag{A5}$$

where the angular part is given by $\mathbf{D}$ tensor. Substituting Eq. (A5) into Eq. (A3), we have

$$\Delta T_I(r) = \frac{2\alpha\rho}{(2\pi)^3} \int_0^\infty (4\pi)^3 k^2 \left[\frac{\cos ka}{(ka)^2} - \frac{\sin ka}{(ka)^3}\right]^2 j_0(kr)\, dk$$

$$= \frac{16\alpha\rho}{a^3 y^3} \int_0^\infty \frac{\sin x (xy\cos xy - \sin xy)^2}{x^5}\, dx, \tag{A6}$$

where $x=kr$ and $y=a/r$. Because the integrand is an even function of x, the lower limit of the integral can be expanded to $-\infty$, and the integral is expanded from real space to complex space. Then, Eq. (A6) becomes

$$\begin{aligned}\Delta T_I(r) &= \frac{8\alpha\rho}{a^3y^3i}\int_{-\infty}^{\infty}\frac{(xy\cos xy-\sin xy)^2}{x^5y^6}e^{ix}\,dx \\ &= \frac{2\alpha\rho}{a^3y^3i}\left[\int_{-\infty}^{\infty}\frac{2x^2y^2+2}{x^5y^6}e^{ix}\,dx\right. \\ &\quad + \int_{-\infty}^{\infty}\frac{x^2y^2+2ixy-1}{x^5y^6}e^{i(1+2y)x}\,dx \\ &\quad \left.+\int_{-\infty}^{\infty}\frac{x^2y^2-2ixy-1}{x^5y^6}e^{i(1-2y)x}\,dx\right] \\ &= \frac{2\alpha\rho}{a^3y^3i}[I_1+I_2+I_3], \end{aligned} \tag{A7}$$

where the three integrals are evaluated using the residue theorem, giving

$$I_1=\frac{(1-12y^2)\pi i}{2}+\frac{2(6y^2-1)i}{3}\epsilon^{-1}+\frac{4i}{3}\epsilon^{-3}, \tag{A8}$$

$$I_2=\frac{(1+2y)^2(4y-1)\pi i}{24}+\frac{(1-6y^2-4y^3)i}{3}\epsilon^{-1} - \frac{2i}{3}\epsilon^{-3}, \tag{A9}$$

$$I_3=\mathrm{sign}(2y-1)\frac{(1-2y)^2(1+4y)\pi i}{24} + \frac{(1-6y^2+4y^3)i}{3}\epsilon^{-1}-\frac{2i}{3}\epsilon^{-3}, \tag{A10}$$

with ϵ an infinitesimal positive variable. Though each integral diverges at the small ϵ limit, the combination of three integrals cancels out all the divergent terms, and the converged sum in Eq. (A7) gives $\Delta T_I(r)$ as

$$\Delta T_I(r)=\begin{cases}0, & r\geqslant 2a \\ \dfrac{\alpha\rho\pi}{6a^3}\left(\dfrac{r}{a}-2\right)^2\left(\dfrac{r}{a}+4\right), & r<2a\end{cases}, \tag{A11}$$

which is a step function at $2a$.

The same approach is applied to the calculation of $\Delta T_D(r)$. First, $\Delta T_D(r)$ is rewritten as

$$\begin{aligned}\Delta T_D(r) &= -\frac{\alpha\rho}{(2\pi)^3}\int d\mathbf{k}\left[4\pi\left(\frac{\cos ka}{k^2a^2}-\frac{\sin ka}{k^3a^3}\right)\right]^2 \\ &\quad\times\left[\left(\frac{3}{x^3}-\frac{1}{x}\right)\sin x-\frac{3}{x^2}\cos x\right] \\ &= -\frac{8\alpha\rho}{a^3y^3}\int_0^{\infty}dx\,\frac{1}{x^4}\left(\frac{3\sin x}{x^3}-\frac{3\cos x}{x^2}-\frac{\sin x}{x}\right) \\ &\quad\times(xy\cos xy-\sin xy)^2 \\ &= -\frac{8\alpha\rho}{a^3y^3}(I_1'-I_2'-I_3'), \end{aligned} \tag{A12}$$

where $I_3'=I_1+I_2+I_3$ is the integral evaluated for $\Delta T_I(r)$. Using the residue theorem, I_1' and I_2' are calculated as

$$\begin{aligned}I_1' &= \frac{3}{8i}\int_{-\infty}^{\infty}dx\left[\frac{2(x^2y^2+1)}{x^7}e^{ix}\right. \\ &\quad + \frac{x^2y^2+2ixy-1}{x^7}e^{i(1+2y)x} \\ &\quad \left.+\frac{x^2y^2-2ixy-1}{x^7}e^{i(1-2y)x}\right] \\ &= \left(\frac{y^6}{12}+\frac{y^5}{10}-\frac{y^3}{24}+\frac{y^2}{64}-\frac{1}{1920}\right)\pi \\ &\quad + \mathrm{sign}(1-2y)\left(\frac{y^6}{12}-\frac{y^5}{10}+\frac{y^3}{24}-\frac{y^2}{64}+\frac{1}{1920}\right)\pi, \end{aligned} \tag{A13}$$

and

$$\begin{aligned}I_2' &= \frac{3}{8}\int_{-\infty}^{\infty}dx\left[\frac{2(x^2y^2+1)}{x^6}e^{ix}\right. \\ &\quad + \frac{x^2y^2+2ixy-1}{x^6}e^{i(1+2y)x} \\ &\quad \left.+\frac{x^2y^2-2ixy-1}{x^6}e^{i(1-2y)x}\right] \\ &= \left(\frac{y^5}{10}-\frac{y^3}{8}+\frac{y^2}{16}-\frac{1}{320}\right)\pi \\ &\quad - \mathrm{sign}(1-2y)\left(\frac{y^5}{10}-\frac{y^3}{8}+\frac{y^2}{16}-\frac{1}{320}\right)\pi, \end{aligned} \tag{A14}$$

where both integrals converge. Substituting I_1', I_2', and I_3' into Eq. (A12), we arrive at

$$\Delta T_D(r)=\begin{cases}-\dfrac{4\pi\alpha\rho}{3r^3}, & r\geqslant 2a \\ -\dfrac{\pi\alpha\rho}{24a^3}\left(\dfrac{6a^2r-r^3}{a^3}\right), & r<2a\end{cases}, \tag{A15}$$

which modifies $1/r^3$ interaction.

APPENDIX B: RENORMALIZATION OF THE DRUDE OSCILLATOR MODEL

To facilitate the analysis of Raman spectroscopy, we present here a simplified derivation of the renormalized polarizability and dipole–induced-dipole (DID) propagator. We follow the same notations used by Cao and Berne.[40]

In an isotropic fluid all particles are identical so that the thermal average of the diagonal elements of the polarizability tensor defines the renormalized polarizability

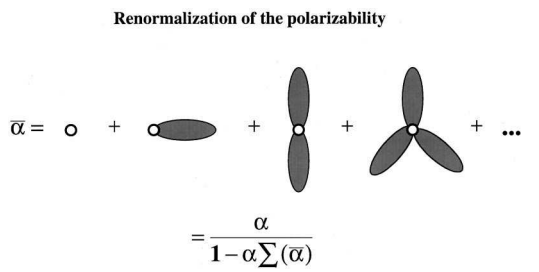

FIG. 14. The many-body expansion and re-summation of the renormalized polarizability. The circle represents the tagged particle and the shaded area represents the self-energy term Σ.

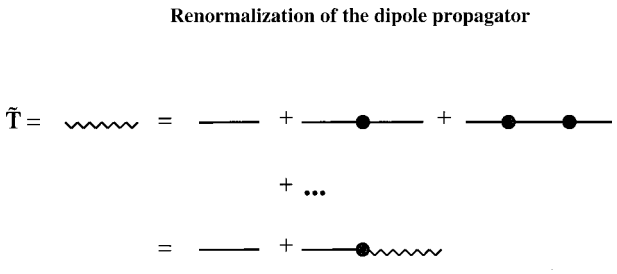

FIG. 16. The Dyson expansion of the renormalized dipole–induced-dipole interaction. Each closed circle represents a dummy particle being integrated with a renormalized polarizability, and each line represents dipole–induced-dipole interaction.

$$\bar{\alpha}=\frac{1}{3N}\langle \mathrm{Tr}\,\mathbf{II}\rangle=\langle \mathbf{II}\rangle_{11}=\sum_{n=0}^{\infty}\alpha^n\langle \mathbf{T}^{n-1}\rangle_{11}, \tag{B1}$$

where the bracket designates the thermal average over disordered liquid configurations. The expansion can be represented by diagrams with open circles as the tagged particles, closed circles as the integrated particles, and lines as the DID propagator. Wherever circles connect two or more otherwise separated subdiagrams, the many-body distribution function is factorized accordingly so that the configurational average associated with subdiagrams can be decoupled from the configurational average of the other parts of the diagram. With this approximation, all the decorations at closed circles (i.e., all the subdiagrams singly connected to the backbone of the diagram) can be removed by replacing α with the renormalized quantity $\bar{\alpha}$. As demonstrated in Fig. 14, the many-body integration of the decorations at the open circle can be re-summed as

$$\begin{aligned}\bar{\alpha}&\approx\alpha+\alpha\left\langle\sum_i \mathbf{T}_{1i}\bar{\alpha}\mathbf{T}_{i1}\right\rangle\alpha\\&\quad+\alpha\left\langle\sum_i \mathbf{T}_{1i}\bar{\alpha}\mathbf{T}_{i1}\right\rangle\alpha\left\langle\sum_j \mathbf{T}_{1j}\bar{\alpha}\mathbf{T}_{j1}\right\rangle\alpha+\cdots\\&=\frac{\alpha}{1-\alpha\Sigma(\bar{\alpha})},\end{aligned} \tag{B2}$$

where Σ is the infinite sum of the simple connected diagrams (i.e., decorations). As shown in Fig. 15, the ring diagrams in the Σ expansion can be re-summed to yield

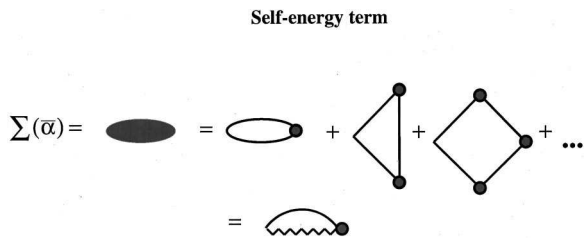

FIG. 15. The ring-diagram expansion of the self-energy Σ. Each closed circle represents a dummy particle being integrated with a renormalized polarizability, and each line represents dipole–induced-dipole interaction.

$$\begin{aligned}\sum(\bar{\alpha})&\approx\langle \mathbf{T}_{1i}\bar{\alpha}\mathbf{T}_{i1}\rangle+\langle \mathbf{T}_{1i}\bar{\alpha}\mathbf{T}_{ij}\bar{\alpha}\mathbf{T}_{j1}\rangle\\&=\rho\bar{\alpha}\int d\mathbf{r}\,\mathbf{T}(\mathbf{r})\bar{\mathbf{T}}(\mathbf{r})g(\mathbf{r})d\mathbf{r},\end{aligned} \tag{B3}$$

where the renormalized propagator $\bar{\mathbf{T}}$ will be explained in the following. Here, the self-energy term Σ is evaluated with the help of $\mathbf{T}$ instead of the Padé approximation or the MSA solution for the dipolar fluid.

Following the definition for $\bar{\alpha}$, we define the off-diagonal element of the polarizability tensor as

$$\Pi_{12}=\left\langle\frac{\alpha\mathbf{T}}{I-\alpha\mathbf{T}}\right\rangle_{12}=\bar{\alpha}\bar{T}(\mathbf{r}_{12})\bar{\alpha}, \tag{B4}$$

where the configurational average excludes indices 1 and 2. First, all the decorations on the backbone can be removed by replacing the polarizability by the renormalized polarizability $\alpha\to\bar{\alpha}$. Second, we keep only diagrams with linear chain structures similar to the Dyson expansion and average over the intermediate particles between indices i and j. Third, the equilibrium average over the n-body distribution is approximately decomposed along the linear chain as

$$\begin{aligned}g(\mathbf{r}_1,\mathbf{r}_2,\mathbf{r}_3,\ldots,\mathbf{r}_n)&\approx g(\mathbf{r}_1-\mathbf{r}_2)g(\mathbf{r}_2-\mathbf{r}_3)\\&\quad\times g(\mathbf{r}_3-\mathbf{r}_4)\cdots g(\mathbf{r}_{n-1}-\mathbf{r}_n)\\&\quad\times g(\mathbf{r}_n-\mathbf{r}_1),\end{aligned} \tag{B5}$$

which extends the Kirkwood approximation beyond the three-body distribution function. With these approximations, we re-sum the expansion of the dipole interaction in Fig. 16 and obtain

$$\begin{aligned}\bar{\mathbf{T}}(\mathbf{k})&\approx\mathbf{T}+\bar{\alpha}\rho\mathbf{T}_g\mathbf{T}_g+(\bar{\alpha}\rho\mathbf{T}_g)^2\mathbf{T}_g+\cdots\\&=\mathbf{T}-\mathbf{T}_g+\frac{\mathbf{T}_g}{1-\bar{\alpha}\rho\mathbf{T}_g},\end{aligned} \tag{B6}$$

where the dipole tensor $\mathbf{T}(\mathbf{r})$ dressed by the pairwise distribution function $g(\mathbf{r})$ is denoted as $\mathbf{T}_g(\mathbf{r})=g(r)\mathbf{T}(\mathbf{r})$. The Fourier transform of the traceless tensor is $\mathbf{T}(\mathbf{k})=-\int j_2(kr)/r^3 d\mathbf{r}\,\mathbf{D}=T(k)\mathbf{D}$, where $j_2(kr)$ is the second-order spherical Bessel function. Similarly, $\bar{\mathbf{T}}_g(\mathbf{k})=-\int g(r)j_2(kr)/r^3 d\mathbf{r}\,\mathbf{D}=T_g(k)\mathbf{D}$. Thus, the renormalized propagator in Eq. (B6) is explicitly evaluated as

$$\overline{\mathbf{T}} \approx \mathbf{T} - \mathbf{T}_g + T_g \frac{\mathbf{D} + 2\sigma(k)\mathbf{I}}{1 - \sigma(k) - 2\sigma^2(k)}. \tag{B7}$$

The transformation back to coordinate space leads to $\overline{\mathbf{T}} = h_D \mathbf{D} + h_I \mathbf{I}$, where the anisotropic part is

$$h_D(r) = -\frac{1}{(2\pi)^3} \int d\mathbf{k}\, j_2(kr) \times \left[T(k) - T_g(k) + \frac{T_g(k)}{1 - \sigma(k) - 2\sigma(k)^2} \right] \tag{B8}$$

and the isotropic part is

$$h_I(r) = \frac{1}{(2\pi)^3} \int d\mathbf{k}\, j_0(kr) \left[T_g(k) \frac{2\sigma(k)}{1 - \sigma(k) - 2\sigma(k)^2} \right], \tag{B9}$$

with $\sigma(k) = \overline{\alpha} \rho T_g(k)$. We solve Eq. (B7) self-consistently with Eq. (B2) to yield the fully renormalized $\overline{\alpha}$ and $\mathbf{T}$. Hence, instead of the Padé approximation or the MSA solution for a dipolar fluid, we explicitly re-sum the diagrams using a decomposition similar to the Kirkwood approximation.

APPENDIX C: MOLECULAR DYNAMICS SIMULATIONS OF LIQUID Xe

Molecular dynamics simulations were carried out using a cubic box containing 108 Xe atoms under the usual periodic boundary condition and minimum image conventions. The interaction between Xe atoms was modeled by a Lennard-Jones potential

$$\phi(r) = 4\epsilon \left[\left(\frac{\sigma}{r} \right)^{12} - \left(\frac{\sigma}{r} \right)^{6} \right] \tag{C1}$$

with parameters $\epsilon = 236.6 k_B$ and $\sigma = 3.88 \rho A$ from the literature.[73] The Lennard-Jones system was equilibrated under reduced temperature $T^* = k_B T/\epsilon = 0.75$ and reduced density $\rho^* = \rho\sigma^3 = 0.85$. The atomic polarizability of Xe varies slightly in literature, and it is taken as $\alpha = 4.16 \rho A^3$ in our simulation, i.e., $\alpha^* = \alpha/\sigma^3 = 0.071$.[79,80] Equations of motion were integrated using the leap-frog algorithm. The reduced time unit is $\sigma\sqrt{m/\epsilon}$, which is 2.7 ps for liquid Xe. All quantities in our simulations are reported in reduced units unless specified otherwise. The time step for MD is 5×10^{-3} reduced time unit. In accord with the spherical cutoff convention, all distance-dependent quantities were calculated within a sphere of a radius of half the box length. The time correlation functions were accumulated with a resolution of 5 time steps. The molecular dynamics simulations were carried out to 10^5 time steps from equilibrium configurations of the liquid. Equilibrium properties, such as the static structure factor and the velocity–velocity correlation function, were calculated and found within good agreement in previously published results.[73,81,82]

As a numerical test, we use the the pair interaction approximation of the total polarizability tensor $\Pi = \Sigma \alpha \mathbf{T} \alpha$ in Eq. (2.5), which leads to the ratio $C_{zzzz} : C_{zyzy} : C_{zzyy} = 4 : 3 : -2$ for an isotropic system. In order to generate an isotropic liquid sample, we compared two numerical methods. The first method is the Ewald summation technique of deLeeuw, Perram, and Smith in their calculation of dielectric constants of polar fluids.[83] In the Ewald summation, the dipole–dipole interaction tensor is modified by the replica of the simulation box and the continuum medium, giving

TABLE I. The absolute intensity and ratio of the three tensor elements of the third-order Raman correlation function in the pair interaction approximation. The ratios in both the Ewald summation method and the spherical cutoff method are nearly the same.

	$C_{zzzz}(0)$	$C_{zyzy}(0)$	$C_{zzyy}(0)$
Ewald summation	0.003 05	0.002 34	−0.001 52
Ratio	4.00	3.07	−2.00
Spherical cutoff	0.002 51	0.001 93	−0.001 26
Ratio	4.00	3.07	−2.00

$$\mathbf{T}_{ij} = \frac{1}{L^3} \nabla\nabla \phi_{\mathrm{Ew}}(R_{ij}/L) - \frac{3}{2\epsilon_s + 1} \frac{4\pi}{3L^3} \mathbf{I}, \tag{C2}$$

where L is the size of the cubic system studied, ϵ_s is the dielectric constant of surrounding medium, and ϕ_{Ew} is the Ewald summation,

$$\phi_{\mathrm{Ew}}(\mathbf{r}) = \sum_{\mathbf{n} \neq 0} \frac{1}{\pi n^2} e^{-(\pi \mathbf{n}/c)^2 + i2\pi \mathbf{n}\cdot\mathbf{r}} + \sum_{\mathbf{n}'} \frac{\mathrm{erfc}(c|\mathbf{r} + \mathbf{n}'|)}{|\mathbf{r} + \mathbf{n}'|} \tag{C3}$$

with c an arbitrary constant and erfc the complementary error function. The constant c in our simulation is taken to be 5.0, which is sufficiently large that the only contribution in the real space part is $n' = 0$ in the second term of ϕ_{Ew}. The number of reciprocal vectors $\mathbf{n}$ used in the first term of ϕ_{Ew} is 63. In the second method, a simple spherical cutoff in the dipole–dipole interaction at half the box length is employed to recover the rotational symmetry of the cubic simulation box. As shown in Table I, though the two methods predict different values, they both give the same intensity ratio $C_{zzzz} : C_{zyzy} : C_{zzyy} = 4 : 3 : -2$, indicating the correct isotropic condition. The Ewald summation has a more reliable theoretical basis; however, due to the constraint on CPU time, we employ the simple spherical cutoff method in the simulations.

APPENDIX D: INITIAL MOMENTS OF THE THIRD-ORDER RAMAN CORRELATION FUNCTION

Because of the many-body polarization in atomic liquids, the renormalized dipole–induced-dipole (DID) interaction tensor, $\overline{\mathbf{T}} = h_D(r)\mathbf{D} + h_I(r)\mathbf{I}$, has both a traceless anisotropic part and a diagonal isotropic part. In this appendix, we derive the initial moments of the correlation functions within the renormalized Drude oscillator model. Components of $\mathbf{T}$ along the arbitrary directions μ and ν (representing x, y, and z) are given as

$$\overline{T}_{\mu\nu} = h_D(r)(3n_\mu n_\nu - \delta_{\mu\nu}) + h_I(r)\delta_{\mu\nu} = 3h_D(r) n_\mu n_\nu + (h_I(r) - h_D(r))\delta_{\mu\nu}, \tag{D1}$$

where n_μ is the μth component of the unit vector and $\delta_{\mu\nu}$ represents the delta function. First the leading order moment of the correlation function is

$$c_0=\langle\overline{T}_{\mu\nu}\overline{T}_{\gamma\lambda}\rangle=\frac{\langle 9h_D^2(r)\rangle_r}{15}(\delta_{\mu\nu}\delta_{\gamma\lambda}+\delta_{\mu\gamma}\delta_{\nu\lambda}+\delta_{\mu\lambda}\delta_{\nu\gamma})+\{2\langle h_D(r)[h_I(r)-h_D(r)]\rangle_r+\langle[h_I(r)-h_D(r)]^2\rangle_r\}\delta_{\mu\nu}\delta_{\gamma\lambda}, \tag{D2}$$

where $\langle f(r)\rangle_r$ represents the radial average, $\langle f(r)\rangle_r=\int f(r)g(r)r^2\,dr$. The three distinct components of the correlation function are

$$\langle\overline{T}_{zz}\overline{T}_{zz}\rangle=\langle h_I^2(r)+\tfrac{4}{5}h_D^2(r)\rangle_r, \tag{D3}$$

$$\langle\overline{T}_{zz}\overline{T}_{yy}\rangle=\langle h_I^2(r)-\tfrac{2}{5}h_D^2(r)\rangle_r, \tag{D4}$$

$$\langle\overline{T}_{zy}\overline{T}_{zy}\rangle=\langle\tfrac{3}{5}h_D^2(r)\rangle_r, \tag{D5}$$

which satisfy the polarization decomposition derived in Sec. II.

Next we derive the second moment of the correlation function. To begin, the first-order time derivative of the renormalized DID tensor is

$$\dot{\overline{T}}_{\mu\nu}=[a_1n_in_\mu n_\nu+a_2(n_\mu\delta_{\nu i}+n_\nu\delta_{\mu i})+a_3n_i\delta_{\mu\nu}]v_i, \tag{D6}$$

where

$$a_1=3h_D'-\frac{6h_D}{r},\quad a_2=\frac{3h_D}{r},\quad a_3=h_I'-h_D', \tag{D7}$$

where the prime represents the spatial derivative with respect to the radial coordinate r, $h_D'=\partial_r h_D$, v_i denotes the ith component of the velocity, and the repeated indices are summed over implicitly. Then, we use Eq. (D7) to derive the second-order moment,

$$\begin{aligned}c_2=\langle\dot{\overline{T}}_{\mu\nu}\dot{\overline{T}}_{\gamma\lambda}\rangle&=\langle\partial_i\overline{T}_{\mu\nu}\partial_i\overline{T}_{\gamma\lambda}\rangle\\&=\frac{1}{m\beta}\left\langle\frac{a_1^2+4a_1a_2}{15}+\frac{2a_2^2}{3}\right\rangle P(\delta\delta)_{\mu\nu\gamma\lambda}+\frac{1}{m\beta}\left\langle a_3^2+\frac{2(2a_2a_3+a_1a_3-a_2^2)}{3}\right\rangle\delta_{\mu\nu}\delta_{\gamma\lambda}\\&=\frac{1}{m\beta}\left\langle\frac{3h_D'^2}{5}+\frac{18h_D^2}{5r^2}\right\rangle_r P(\delta\delta)-\frac{1}{m\beta}\mu\nu\gamma\lambda+\left\langle h_I'^2-h_D'^2-\frac{6h_D^2}{r^2}\right\rangle_r\delta_{\mu\nu}\delta_{\gamma\lambda},\end{aligned} \tag{D8}$$

where operator P represents the permutation of the indices and $P(\delta\delta)_{\mu\nu\gamma\lambda}=\delta_{\mu\nu}\delta_{\gamma\lambda}+\delta_{\mu\gamma}\delta_{\nu\lambda}+\delta_{\mu\lambda}\delta_{\nu\gamma}$. The three tensor components are

$$\langle\dot{\overline{T}}_{zz}\dot{\overline{T}}_{zz}\rangle=\left\langle\frac{4}{5}\left(h_D'^2+6\frac{h_D^2}{r^2}\right)+h_I'^2\right\rangle_r, \tag{D9}$$

$$\langle\dot{\overline{T}}_{zz}\dot{\overline{T}}_{yy}\rangle=\left\langle-\frac{2}{5}\left(h_D'^2+6\frac{h_D^2}{r^2}\right)+h_I'^2\right\rangle_r, \tag{D10}$$

$$\langle\dot{\overline{T}}_{zy}\dot{\overline{T}}_{zy}\rangle=\left\langle\frac{3}{5}\left(h_D'^2+6\frac{h_D^2}{r^2}\right)\right\rangle_r, \tag{D11}$$

which also satisfy the polarization decomposition relation.

Finally, we derive the fourth-order moment of the correlation functions. To begin, we write the second-order time derivative of the polarizability tensor as

$$\ddot{\overline{T}}_{\mu\nu}=\frac{d}{dt}(\partial_j\overline{T}_{\mu\nu}v_j)=(\partial_i\overline{T}_{\mu\nu})\frac{F_i}{m}+v_iv_j\partial_{ij}^2\overline{T}_{\mu\nu}, \tag{D12}$$

where $\partial_{ij}^2=\partial_i\partial_j$, F_i represents the ith component of the force, which is related to the potential $U(r)$ by $F_i=-\partial_iU(r)$. From Eq. (D12), the fourth-order moment becomes

$$\begin{aligned}\langle\ddot{\overline{T}}_{\mu\nu}\ddot{\overline{T}}_{\gamma\lambda}\rangle&=\langle\partial_{ij}^2\overline{T}_{\mu\nu}\partial_{kl}^2\overline{T}_{\gamma\lambda}\rangle\langle v_iv_jv_kv_l\rangle+\left\langle\partial_{ij}^2\overline{T}_{\mu\nu}\frac{F_k}{m}\partial_k\overline{T}_{\gamma\lambda}\right\rangle\langle v_iv_j\rangle+\left\langle\partial_{kl}^2\overline{T}_{\gamma\lambda}\frac{F_i}{m}\partial_i\overline{T}_{\mu\nu}\right\rangle\langle v_kv_l\rangle\\&\quad+\frac{1}{m^2}\langle F_i\partial_i\overline{T}_{\mu\nu}F_k\partial_k\overline{T}_{\gamma\lambda}\rangle\\&=A_1+A_2+A_3+A_4,\end{aligned} \tag{D13}$$

which is separated into four parts. These four parts in Eq. (D13) are explicitly evaluated as

$$\begin{aligned}A_1&=\left(\frac{1}{m\beta}\right)^2\langle\partial_{ij}^2\overline{T}_{\mu\nu}\partial_{kl}^2\overline{T}_{\gamma\lambda}\rangle P(\delta\delta)_{ijkl}\\&=\left(\frac{1}{m\beta}\right)^2(\langle\partial_i^2\overline{T}_{\mu\nu}\partial_j^2\overline{T}_{\gamma\lambda}\rangle+2\langle\partial_{ij}^2\overline{T}_{\mu\nu}\partial_{ij}^2\overline{T}_{\gamma\lambda}\rangle),\end{aligned} \tag{D14}$$

$$\begin{aligned}A_2&=\frac{k_BT}{m^2}\langle F_k\partial_i^2\overline{T}_{\mu\nu}\partial_k\overline{T}_{\gamma\lambda}\rangle\\&=-\left(\frac{1}{m\beta}\right)^2(\langle\partial_i^2\partial j\overline{T}_{\mu\nu}\partial_j\overline{T}_{\gamma\lambda}\rangle+\langle\partial_i^2\overline{T}_{\mu\nu}\partial_j^2\overline{T}_{\gamma\lambda}\rangle),\end{aligned} \tag{D15}$$

$$A_3=-\left(\frac{1}{m\beta}\right)^2(\langle\partial_i\overline{T}_{\mu\nu}\partial_j^2\partial_i\overline{T}_{\gamma\lambda}\rangle+\langle\partial_i^2\overline{T}_{\mu\nu}\partial_j^2\overline{T}_{\gamma\lambda}\rangle), \tag{D16}$$

and

$$\begin{aligned}A_4&=-\frac{k_BT}{m^2}\langle\partial_i(\partial_i\overline{T}_{\mu\nu}F_j\partial_j\overline{T}_{\gamma\lambda})\rangle\\&=-\frac{k_BT}{m^2}[\langle\partial_i^2\overline{T}_{\mu\nu}F_j\partial_j\overline{T}_{\gamma\lambda}\rangle+\langle\partial_i\overline{T}_{\mu\nu}\partial_i(F_j\partial_j\overline{T}_{\gamma\lambda})\rangle+\langle\partial_i\overline{T}_{\mu\nu}F_j\partial_{ij}\overline{T}_{\gamma\lambda}\rangle]\\&=\frac{1}{m\beta}\langle\partial_i\overline{T}_{\mu\nu}\partial_j\overline{T}_{\gamma\lambda}\Omega_{ij}^2\rangle+\left(\frac{1}{m\beta}\right)^2\langle\partial_{ij}(\partial_i\overline{T}_{\mu\nu}\partial_j\overline{T}_{\gamma\lambda})\rangle.\end{aligned} \tag{D17}$$

Here, Ω_{ij} is the curvature,

$$\Omega_{ij}^2=\frac{1}{m}\partial_{ij}U(r)=c(r)\delta_{ij}+d(r)n_in_j \tag{D18}$$

with $c(r)=\partial_r U(r)/(mr)$ and $d(r)=\partial_r^2 U(r)/m-\partial_r U(r)/(mr)$. Substituting the above-given four terms into Eq. (D13), the fourth-order moment is the sum of two terms

$$c_4=\langle \ddot{\overline{T}}_{\mu\nu}\ddot{\overline{T}}_{\gamma\lambda}\rangle=\frac{1}{m\beta}\langle \partial_i\overline{T}_{\mu\nu}\partial_j\overline{T}_{\gamma\lambda}\Omega_{ij}^2\rangle + 3\left(\frac{1}{m\beta}\right)^2\langle \partial_i^2\overline{T}_{\mu\nu}\partial_j^2\overline{T}_{\gamma\lambda}\rangle. \tag{D19}$$

The first term is further simplified to

$$\begin{aligned}\langle \partial_i\overline{T}_{\mu\nu}\partial_j\overline{T}_{\gamma\lambda}\Omega_{ij}^2\rangle &= \langle c(r)\,\delta_{ij}\partial_i\overline{T}_{\mu\nu}\partial_j\overline{T}_{\gamma\lambda} + d(r)n_in_j\partial_i\overline{T}_{\mu\nu}\partial_j\overline{T}_{\gamma\lambda}\rangle \\ &= \langle c(r)[\tfrac{1}{15}(a_1^2+4a_1a_2 + 10a_2^2)P(\delta\delta)_{\mu\nu\gamma\lambda}+(a_3^2+\tfrac{2}{3}(2a_2a_3 + a_1a_3-a_2^2))\delta_{\mu\nu}\delta_{\gamma\lambda}]\rangle_r+\langle d(r) \\ &\quad\times[\tfrac{1}{15}(a_1+2a_2)^2P(\delta\delta)_{\mu\nu\gamma\lambda}+(a_3^2 + \tfrac{2}{3}(a_1a_3+2a_2a_3))\delta_{\mu\nu}\delta_{\gamma\lambda}]\rangle_r .\end{aligned} \tag{D20}$$

For the second part, we first evaluate $\partial_{ij}\overline{T}_{\mu\nu}$,

$$\begin{aligned}\partial_{ij}\overline{T}_{\mu\nu} &= \partial_i[a_1n_jn_\mu n_\nu+a_2(n_\mu\delta_{\nu j}+n_\nu\delta_{\mu j})+a_3n_j\delta_{\mu\nu}] \\ &= \left[\left(a_1'-\frac{3a_1}{r}\right)n_\mu n_\nu+\left(a_3'-\frac{a_3}{r}\delta_{\mu\nu}\right)\right]n_in_j \\ &\quad+\left(\frac{a_1}{r}n_\mu n_\nu+\frac{a_3}{r}\delta_{\mu\nu}\right)\delta_{ij}+\frac{a_1}{r}(\delta_{\mu i}n_\nu \\ &\quad+\delta_{\nu i}n_\mu)n_j+\left(a_2'-\frac{a_2}{r}\right)(\delta_{\mu j}n_\nu+\delta_{\nu j}n_\mu)n_i \\ &\quad+\frac{a_2}{r}(\delta_{\mu i}\delta_{\nu j}+\delta_{\mu j}\delta_{\nu i}),\end{aligned} \tag{D21}$$

so that

$$\begin{aligned}&\langle \partial_{ij}\overline{T}_{\mu\nu}\partial_{ij}\overline{T}_{\gamma\lambda}\rangle \\ &= \frac{3}{5}\left\langle 12\frac{h_D^2}{r^4}+4\frac{h_Dh_D'}{r^3}-6\frac{h_D'^2}{r^2}+h_D''^2\right\rangle_r \\ &\quad\times P(\delta)_{\mu\nu\gamma\lambda}+\left\langle -24\frac{h_D^2}{r^4}+12\frac{h_Dh_D'}{r^3}-2\frac{h_D'^2}{r^2}-h_D''^2\right. \\ &\quad\left.+\frac{h_I'^2}{r^2}+h_I''^2\right\rangle_r\delta_{\mu\nu}\delta_{\gamma\lambda}+6\left\langle 3\frac{h_D^2}{r^4}-4\frac{h_Dh_D'}{r^3}+2\frac{h_D'^2}{r^2}\right\rangle_r \\ &\quad\times(\delta_{\mu\gamma}\delta_{\nu\lambda}+\delta_{\mu\lambda}\delta_{\nu\gamma}).\end{aligned} \tag{D22}$$

Substituting Eqs. (D20) and (D22) into Eq. (D19), we have the explicit expression of the fourth-moment of the correlation function. As an example, we give the C_{zzzz} component as

$$\begin{aligned}&\langle \ddot{\overline{T}}_{zz}\ddot{\overline{T}}_{zz}\rangle \\ &= \frac{1}{m\beta}\left\{\left\langle c(r)\left[\frac{4}{5}\left(h_D'^2+6\frac{h_D^2}{r^2}\right)+h_I'^2\right]\right\rangle_r\right. \\ &\quad\left.+\left\langle d(r)\left(\frac{4}{5}h_D'^2+h_I'^2\right)\right\rangle_r\right\} \\ &\quad\times 3\left(\frac{1}{m\beta}\right)^2\left\langle\frac{4}{5}\left(h_D''^2+14\frac{h_D'^2}{r^2}-36\frac{h_D'h_D''}{r^3}+42\frac{h_D^2}{r^4}\right)\right. \\ &\quad\left.+\left(h_I''^2+2\frac{h_I'^2}{r^2}\right)\right\rangle_r .\end{aligned} \tag{D23}$$

We can show that all the fourth-order moments also satisfy the polarization decomposition relation.

APPENDIX E: ENERGY GAP CORRELATION FUNCTION

A key quantity in solvation dynamics is the energy gap correlation function

$$C(t)=\left\langle \sum_i \phi[\mathbf{r}_i(t)-\mathbf{r}_0(t)]\middle|\sum_j \phi[\mathbf{r}_j(0)-\mathbf{r}_0(0)]\right\rangle, \tag{E1}$$

where ϕ is the interaction potential or the force between the solvent and solute, $\mathbf{r}_i$ is the coordinate of the ith solvent particle, and $\mathbf{r}_0$ is the coordinate of the solute particle. Many experimental measurements can be related to the energy gap correlation function, which in proper forms describes energy relaxation and dephasing (electronic or nuclear), solvation dynamics, and charge transfer. The energy gap correlation function has been evaluated within hydrodynamic theory by Skinner, Fayer, Banchi, and their co-workers. Here we compare their expressions from the unified perspective of dynamic decomposition.

1. Gaussian factorization

We begin by writing the correlation function as

$$\begin{aligned}C(t) &= \int d\mathbf{r}\,d\mathbf{r}'\,d\mathbf{r}_0\,d\mathbf{r}_0'P(\mathbf{r}_0,\mathbf{r},\mathbf{r}_0',\mathbf{r}',t) \\ &\quad\times\phi(\mathbf{r}-\mathbf{r}_0)\phi(\mathbf{r}'-\mathbf{r}_0'),\end{aligned} \tag{E2}$$

where P is the joint density distribution function defined earlier. The simple Gaussian factorization scheme results in $P(\mathbf{r}_0,\mathbf{r},\mathbf{r}_0',\mathbf{r}',t)\approx\rho G_s(\mathbf{r}_0,\mathbf{r}_0',t)G(\mathbf{r},\mathbf{r}',t)g(\mathbf{r}-\mathbf{r}_0)g(\mathbf{r}'-\mathbf{r}_0')$, where G_s is the self-correlation function for the solute and G is the van Hove function for the solvent. Substituting this expression into the correlation function, we obtain

$$\begin{aligned}C(t) &= \int d\mathbf{r}\,d\mathbf{r}'\,d\mathbf{r}_0\,d\mathbf{r}_0'G_s(\mathbf{r}_0,\mathbf{r}_0',t) \\ &\quad\times G(\mathbf{r},\mathbf{r}',t)\phi_g(\mathbf{r}-\mathbf{r}_0)\phi_g(\mathbf{r}'-\mathbf{r}_0') \\ &= \frac{\rho}{(2\pi)^3}\int d\mathbf{k}\,\phi_g^2(\mathbf{k})F(\mathbf{k},t)F_s(\mathbf{k},t),\end{aligned} \tag{E3}$$

where $F(\mathbf{k},t)$ is the intermediate scattering function of the solvent and $F_s(\mathbf{k},t)$ the self-intermediate scattering function

of the solute. The dressed interaction potential is defined as $\phi_g(\mathbf{r})=\phi(\mathbf{r})g(\mathbf{r})$ with g the solvent–solute pair correlation function. Equation (E3) has been obtained by Hills using various superposition approximations. If ϕ is the potential responsible for the solute–solvent structure, we then apply the mean spherical approximation and replace $-\beta\phi(\mathbf{r})g(\mathbf{r})$ with the direct correlation function $c(\mathbf{r})$. With this approximation, Eq. (E3) becomes

$$C(t)=\frac{\rho(k_BT)^2}{(2\pi)^3}\int d\mathbf{k}\,c^2(\mathbf{k})F(\mathbf{k},t)F_s(\mathbf{k},t), \tag{E4}$$

which has been used by Banchi, Cherayil, Fayer, and their co-workers for calculating vibrational relaxation.[47,48]

The Gaussian factorization scheme starts to fail at short times and does not recover the equilibrium distribution at the initial time. To improve the accuracy of the Gaussian factorization, one has to correct the initial value of the correlation function while maintaining the structure of the dynamic decomposition. One possible way to include the initial-value correction is to rewrite Eq. (E3) as

$$C(t)=\rho\int d\mathbf{r}\,d\mathbf{r}'\,G(\mathbf{r},\mathbf{r}',t)\times\phi(\mathbf{r}-\mathbf{r}_0)\phi(\mathbf{r}'-\mathbf{r}_0)\frac{\rho(\mathbf{r},\mathbf{r}',\mathbf{r}_0)}{\rho(\mathbf{r},\mathbf{r}')}, \tag{E5}$$

where the solute motion is not included. Here, $\rho(\mathbf{r},\mathbf{r}',\mathbf{r}_0)$ is the density–density correlation function in the presence of the solute, and $\rho(\mathbf{r},\mathbf{r}')$ is the density–density correlation function without the presence of the solute. The denominator $\rho(\mathbf{r},\mathbf{r}')$ cancels the van Hove function in the numerator at the initial time, thus recovering the exact initial value. With the Kirkwood decomposition approximation of $\rho(\mathbf{r},\mathbf{r}',\mathbf{r}_0)$, Eq. (E5) recovers the simple Gaussian factorization expression in Eq. (E3). Similar corrections can also be introduced in Fourier space.

2. Dynamic Kirkwood superposition

We follow the method used by the Skinner group. First, the energy gap correlation function is separated into the two-particle and three-particle contributions $C_2(t)$ and $C_3(t)$, $C(t)=C_2(t)+C_3(t)$. The two-body contribution is written as

$$C_2(t)=\sum_i\langle\phi[\mathbf{r}_i(t)-\mathbf{r}_0(t)]\phi[\mathbf{r}_i(0)-\mathbf{r}_0(0)]\rangle=\rho\int d\mathbf{r}_1\,d\mathbf{r}_1'g(\mathbf{r}_1)\phi(\mathbf{r}_1)G(\mathbf{r}_1,\mathbf{r}_1',t)\phi(\mathbf{r}_1'), \tag{E6}$$

where $\mathbf{r}_1$ and $\mathbf{r}_1'$ are the solvent–solute separations at time zero and time t, respectively, and $G(\mathbf{r}_1,\mathbf{r}_1',t)$ is the Green's function for the solvent–solute motion. If the solute is immobile, Eq. (E6) is exact because the center-of-mass motion is irrelevant. The three-particle contribution involves two solvent particles and the solute,

$$C_3(t)=\sum_{i\neq j}\langle\phi[\mathbf{r}_i(t)-\mathbf{r}_0(t)]\phi[\mathbf{r}_j(0)-\mathbf{r}_0(0)]\rangle=\rho^2\int d\mathbf{r}_1\,d\mathbf{r}_2\,d\mathbf{r}_1'\,d\mathbf{r}_2'\,g(\mathbf{r}_1,\mathbf{r}_2,\mathbf{r}_{12})\times\phi(\mathbf{r}_2)G(\mathbf{r}_1,\mathbf{r}_2,\mathbf{r}_1',\mathbf{r}_2',t)\phi(\mathbf{r}_1'), \tag{E7}$$

where $\mathbf{r}'$ is the solvent–solute separation at time t and $\mathbf{r}$ is the solvent–solute separation at the initial time. The three-body Green's function is factorized into the two-body solvent–solute Green's function, and the Kirkwood superposition approximation is used to evaluate the three-body distribution function. Then, we have

$$C_3(t)\approx\rho^2\int d\mathbf{r}_1\,d\mathbf{r}_2\,d\mathbf{r}_1'\,\phi(\mathbf{r}_2)g(\mathbf{r}_1)g(\mathbf{r}_2)g(\mathbf{r}_{12})\times G(\mathbf{r}_1,\mathbf{r}_1',t)\phi(\mathbf{r}_1'), \tag{E8}$$

which can be understood as a different dynamic factorization scheme. As shown by the Skinner group, the above-given expression for $C_3(t)$, in combination with $C_2(t)$, predicts the energy gap correlation function with remarkable accuracy. The prediction of vibrational relaxation rate using this approach is reliable and leads to simple physical interpretation.[45,46,84]

Both dynamic Kirkwood superposition and Gaussian factorization are designed to decompose multiple correlation functions to linear correlation functions. The simple Gaussian factorization scheme takes into account the solvent–solvent density fluctuation but ignores the solute–solvent dynamic effect, whereas the dynamic Kirkwood superposition takes into account the solute–solvent dynamics at low to intermediate densities but ignores the solvent–solvent dynamics at high densities.[85] Therefore, the first scheme works better for weak solvent–solute interactions and the second scheme works better for strong solvent–solute interactions.

[1] B. J. Berne and R. Pecora, *Dynamic Light Scattering* (Wiley-Interscience, New York, 1976).
[2] G. R. Fleming, *Chemical Applications of Ultrafast Spectroscopy* (Oxford University Press, London, 1986).
[3] S. Mukamel, *The Principles of Nonlinear Optical Spectroscopy* (Oxford University Press, London, 1995).
[4] K. D. Rector, J. R. Engholm, J. R. Hill, D. J. Mayers, R. Hu, S. G. Boxer, D. D. Dlott, and M. D. Fayer, J. Phys. Chem. **102**, 331 (1998).
[5] P. Hamm, M. Lim, M. Asplund, and R. M. Hochstrasser, Chem. Phys. Lett. **301**, 167 (1999).
[6] P. Vohringer, D. C. Arnett, T.-S. Yang, and N. F. Scherer, Chem. Phys. Lett. **237**, 387 (1995).
[7] C. J. Brennan and K. A. Nelson, J. Chem. Phys. **107**, 9691 (1997).
[8] R. F. Loring and S. Mukamel, J. Chem. Phys. **83**, 2116 (1985).
[9] Y. Tanimura and S. Mukamel, J. Chem. Phys. **99**, 9496 (1993).
[10] K. Okumura and Y. Tanimura, J. Chem. Phys. **105**, 7294 (1996).
[11] J. A. Leegwater and S. Mukamel, J. Chem. Phys. **102**, 2365 (1995).
[12] S. Mukamel, Annu. Rev. Phys. Chem. **51**, 691 (2000).
[13] M. Cho, in *Advances in Multi-Photon Processes and Spectroscopy*, edited by S. H. Lin, A. A. Villaeys, and Y. Fujimura (World Scientific, Singapore, 1999).
[14] K. Tominaga and K. Yoshihara, Phys. Rev. Lett. **74**, 3061 (1995).
[15] T. Steffen and K. Duppen, Phys. Rev. Lett. **76**, 1224 (1996).
[16] T. Steffen and K. Duppen, J. Chem. Phys. **106**, 3854 (1997).
[17] D. J. Ulness, J. C. Kirkwood, and A. C. Albrecht, J. Chem. Phys. **108**, 3897 (1998).
[18] A. Tokmakoff, M. J. Lang, D. S. Larsen, G. R. Fleming, V. Chernyak, and S. Mukamel, Phys. Rev. Lett. **79**, 2702 (1997).

[374319] W. Zhou and J. C. Wright, Phys. Rev. Lett. **84**, 1411 (2000).
[20] V. Astinov, K. J. Kubarych, C. J. Milne, and R. J. D. Miller, Chem. Phys. Lett. **327**, 334 (2000).
[21] O. Golonzka, N. Demirdoven, M. Khalil, and A. Tokmakoff, J. Chem. Phys. **113**, 9893 (2000).
[22] D. A. Blank, G. R. Fleming, M. Cho, and A. Tokmakoff, in *Ultrafast Infrared and Raman Spectroscopy*, edited by M. D. Fayer, 1999.
[23] L. Kaufman, D. A. Blank, and G. R. Fleming, J. Chem. Phys. **114**, 2312 (2001).
[24] J. P. McTague and G. Birnbaum, Phys. Rev. Lett. **21**, 661 (1968).
[25] W. M. Gelbart, Adv. Chem. Phys. **26**, 1 (1974).
[26] D. W. Oxtoby and W. M. Gelbart, Mol. Phys. **29**, 1569 (1975).
[27] J. M. Deutch, Annu. Rev. Phys. Chem. **24**, 301 (1973).
[28] D. E. Sullivan and J. M. Deutch, J. Chem. Phys. **62**, 2130 (1975).
[29] M. S. Wertheim, J. Chem. Phys. **55**, 4291 (1971).
[30] D. F. Calef and P. G. Wolynes, J. Chem. Phys. **78**, 4145 (1983).
[31] P. G. Wolynes, J. Chem. Phys. **86**, 5133 (1987).
[32] D. Kivelson and T. Keyes, J. Chem. Phys. **57**, 4599 (1972).
[33] B. M. Ladanyi and T. Keyes, Mol. Phys. **33**, 1063 (1977); **33**, 1099 (1977).
[34] P. A. Madden and D. J. Tildesley, Mol. Phys. **55**, 969 (1985).
[35] L. C. Geiger and B. M. Ladanyi, J. Chem. Phys. **87**, 191 (1987).
[36] H. Stassen and W. A. Steele, J. Chem. Phys. **110**, 7382 (1999).
[37] G. Stell, G. N. Patey, and J. S. Hoye, Adv. Chem. Phys. **48**, 183 (1981).
[38] D. Chandler, K. S. Schweizer, and P. G. Wolynes, Phys. Rev. Lett. **49**, 1100 (1982).
[39] R. M. Stratt, J. Chem. Phys. **80**, 5764 (1984).
[40] J. Cao and B. J. Berne, J. Chem. Phys. **99**, 6998 (1993).
[41] L. R. Pratt, Mol. Phys. **40**, 347 (1980).
[42] J. S. Hoye and G. Stell, J. Chem. Phys. **73**, 461 (1980).
[43] P. N. Butcher and D. Cotter, *The Elements of Nonlinear Optics* (Cambridge University Press, Cambridge, 1990).
[44] A. Tokmakoff, J. Chem. Phys. **105**, 1 (1996).
[45] J. G. Saven and J. L. Skinner, J. Chem. Phys. **99**, 4391 (1993).
[46] S. A. Egorov and J. L. Skinner, J. Chem. Phys. **112**, 275 (2000).
[47] B. J. Cherayil and M. D. Fayer, J. Chem. Phys. **107**, 7642 (1997).
[48] D. J. Meyers, M. Shigeiwa, M. D. Fayer, and B. J. Cherayil, J. Phys. Chem. B **104**, 2402 (2000).
[49] W. Gotze, in *Liquids, Freezing and the Glass Transition*, edited by J. P. Hansen, D. Levesque, and J. Zinn-Justin (North-Holland, Amsderdam, 1991).
[50] J. P. Hansen and I. R. McDonald, *Theory of Simple Liquids* (Academic, New York, 1990).
[51] U. Balucani and M. Zoppi, *Dynamics of the Liquid State* (Oxford University Press, New York, 1994).
[52] P. A. Madden, Mol. Phys. **36**, 365 (1978).
[53] A. Ladd, T. A. Litovitz, and C. J. Montrose, J. Chem. Phys. **71**, 4242 (1979).
[54] U. Balucani and M. Zoppi, *Dynamics of the Liquid State* (Oxford University Press, New York, 1994), Appendix J.
[55] G. Seeley and T. Keyes, J. Chem. Phys. **91**, 5581 (1989).
[56] M. Cho, G. R. Fleming, S. Saito, I. Ohmine, and R. Stratt, J. Chem. Phys. **100**, 6672 (1994).
[57] B. M. Ladanyi and S. Klein, J. Chem. Phys. **105**, 1552 (1996).
[58] J. T. Kindt and C. A. Schmuttenmaer, J. Chem. Phys. **106**, 4389 (1997).
[59] S. Saito and I. Ohmine, J. Chem. Phys. **108**, 240 (1998).
[60] R. L. Murry, J. T. Fourkas, and T. Keyes, J. Chem. Phys. **109**, 2814 (1998).
[61] R. L. Murry, J. T. Fourkas, W. Li, and T. Keyes, Phys. Rev. Lett. **83**, 3550 (1999).
[62] T. Keyes and J. T. Fourkas, J. Chem. Phys. **112**, 287 (2000).
[63] A. Ma and R. M. Stratt, Phys. Rev. Lett. **85**, 1004 (2000).
[64] T. I. C. Jansen, J. G. Snijders, and K. Duppen, J. Chem. Phys. **113**, 307 (2000).
[65] H. Metiu, D. W. Oxtoby, and K. F. Freed, Phys. Rev. A **15**, 361 (1977).
[66] D. W. Oxtoby, Adv. Chem. Phys. **47**, 487 (1981).
[67] M. Maroncelli, J. MacInnis, and G. R. Fleming, Science **243**, 1674 (1989).
[68] B. J. Berne, M. E. Tuckerman, J. E. Straub, and A. L. R. Bug, J. Chem. Phys. **93**, 5084 (1990).
[69] J. S. Bader, B. J. Berne, E. Pollak, and P. Hanggi, J. Chem. Phys. **104**, 1111 (1996).
[70] B. J. Schwartz, E. R. Bittner, O. V. Prezhdo, and P. J. Rossky, J. Chem. Phys. **104**, 5942 (1996).
[71] S. A. Egorov and J. L. Skinner, Chem. Phys. **105**, 7047 (1996).
[72] R. B. Williams and R. F. Loring, J. Chem. Phys. **110**, 10899 (1999).
[73] J. P. Boon and S. Yip, *Molecular Hydrodynamics* (McGraw–Hill, New York, 1980).
[74] Y. X. Yan and K. A. Nelson, J. Chem. Phys. **87**, 6240 (1987); **87**, 6257 (1987).
[75] M. Berg, J. Phys. Chem. **102**, 17 (1998).
[76] J. Schofield, R. Lim, and I. Oppenheim, Physica A **181**, 89 (1992).
[77] E. Zaccarelli, G. Foffi, F. Sciortino, P. Tartaglia, and K. A. Dawson, Europhys. Lett. **55**, 157 (2001).
[78] T. Keyes and I. Oppenheim, Phys. Rev. A **9**, 937 (1973).
[79] J. A. Chapman, D. C. Finnimore, and B. L. Smith, Phys. Rev. Lett. **21**, 1306 (1968).
[80] E. Mathias, C. A. Crommelon, and J. J. Meihuitzen, Physica (Amsterdam) **4**, 1200 (1937).
[81] B. J. Berne, *Statistical Mechanics, Part B: Time-dependent Processes* (Plenum, New York, 1977).
[82] M. P. Allen and D. J. Tildesley, *Computer Simulation of Liquids* (Oxford Science, Oxford, 1989).
[83] S. W. de Leeus, J. W. Perram, and E. R. Smith, Proc. R. Soc. London, Ser. A **373**, 57 (1980).
[84] V. S. Vikhrenko, D. Schwartzer, and J. Schroeder, Phys. Chem. Chem. Phys. **3**, 1000 (2001).
[85] B. M. Ladanyi, A. Barreau, and B. Dumon, Mol. Phys. **76**, 735 (1992).